rothymidine (TFT). We also plated 1.6 cells/well without TFT to determine plating efficiency. All plates were incubated at 37 °C in a humidified atmosphere of 5% CO_2 in air. After 14 days, we scored colonies on the PE plates and the normal-growing (NG) *TK* mutants on the TFT plates, then re-fed the plates containing TFT with fresh TFT, incubated them for an additional 14 days, and scored them for slow-growing (SG) *TK* mutants. Mutation frequencies, relative survival (RS), and relative suspension growth (RSG) were calculated as previously described [23]. The data of mutant frequencies were statistically analyzed by Omori's method, which consists of a modified Dunnett's procedure for identifying clear negative, a Simpson–Margolin procedure for detecting downturn data, and a trend test to evaluate the dose-dependency [27].

2.3. LOH analysis of TK mutations by polymerase chain reaction (PCR)

To avoid analyzing identical mutants, we performed an additional *TK* mutation assay and isolated *TK* mutants from independent culture after a 4 h treatment with 2.5 mM $KBrO_3$. We confirmed the phenotype of the *TK* mutant clones by re-challenging them with TFT medium. We also determined the growth rate of the clones and confirmed whether they were NG or SG mutants.

Genomic DNA was extracted from the *TK* mutant cells and used as a template for PCR. We conducted the PCR-based LOH analysis of the human *TK* gene as described previously [28]. A set of primers was used to each amplify the parts of exons 4 and 7 of the *TK* gene that is heterozygous for frame shift mutations. A third primer set for amplifying parts of the β-globin was also used as the internal control. We applied quantitative-multiple PCR for co-amplification of the three regions. The PCR products were analyzed with an ABI310 genetic analyzer (PE Biosystems, Chiba, Japan), and were classified into "no LOH", "hemizygous (hemi-) LOH", or "homozygous (homo-) LOH". To determine the extent of the LOH, we analyzed 10 microsatellite loci on chromosome 17q by PCR-based LOH analysis [28]. The results were processed by GenoTyper™ software (PE Biosystems, Chiba, Japan) according to the manufacturer's guidelines.

2.4. Gene expression analysis

Total RNA was isolated from the TK6 cells after 4 h treatment with 2.5 mM $KBrO_3$ and was purified by RNeasy columns (Qiagen, Valencia, CA). We conducted a single cDNA synthesis, cRNA labeling, and cRNA fragmentation according to the manufacturer's recommendations (Affymetrix Inc., Santa Clara, CA) and employed Affymetrix GeneChip Expression analysis. The hybridization mixture for each sample was hybridized to an Affymetrix U133A human genome array. We processed the scanned data using Microarray Suite Software Version 5.0 (Affymetrix Inc., Santa Clara, CA) and imported the data into GeneSpring software (Silicon Genetics, Redwood City, CA). Signal intensity was normalized by per-gene and per-chip, and the ratios were calculated by normalizing $KBrO_3$ sample to the corresponding control sample. We used intensity-dependent (step-wise) selection of significant changes with higher cut-off value for lower signal intensity (1.75-, 2.0-, 2.25-, 2.5-, and 3.5-fold for genes intensity range of >1000, 500–1000, 100–500, 50–100, and 10–50, respectively), and up-regulated genes with a presence call in $KBrO_3$ sample, whereas down-regulated genes with a presence call in the control sample.

3. Results

3.1. Cytotoxicity and genotoxicity of $KBrO_3$

$KBrO_3$ exerted strong and concentration-dependent cytotoxicity in TK6 cells (Fig. 1). It induced approximately 50% cytotoxicity (51% RSG and 44% RS) at 2.5 mM. To investigate whether $KBrO_3$ directly causes DNA damage, we conducted the COM assay. Induction of COM tail after the treatment of in alkaline version was statistically significant 2.5 and 5 mM. In the neutral COM assay, the induction was observed form the lower concentration (Fig. 1). Because the neutral COM is thought to be associated with DNA double strand breaks (DSBs) [29], this result indicates that $KBrO_3$ directly causes DNA damage including DSBs. $KBrO_3$ also induced MN and *TK* mutation in a concentration-dependent manner and their inductions were statistically significant (Fig. 1). At the maximum concentration, it induced both MN and *TK* mutation frequencies about 30 times the control values. Two distinct phenotypic classes of *TK* mutants were generated: NG mutants grew at the same rate as the wild type (doubling time 13–17 h), and SG mutants grew at a slower rate (doubling time > 21 h). NG mutants result from intragenic mutations, while SG mutants result from gross changes (extending beyond the *TK* gene) [20]. $KBrO_3$ predominantly induced SG mutants (Fig. 1), implying that $KBrO_3$ treatment predominantly causes gross structural changes, but not small genetic alterations such as point mutations.

3.2. Molecular analysis of TK mutants

The *TK* mutants were randomly isolated from independent cultures treated with 2.5 mM $KBrO_3$ for 4 h. Table 1 shows the cytotoxicity (RSG), mutation frequency, and proportion of SG mutants induced by $KBrO_3$. We subjected 40 induced mutants to LOH analysis. Of those, 32 (80%) were SG mutants, which corresponded closely to the percentage of SG mutants induced in the assay (74.1%), indicating that the result of LOH analysis reflected the character of the induced

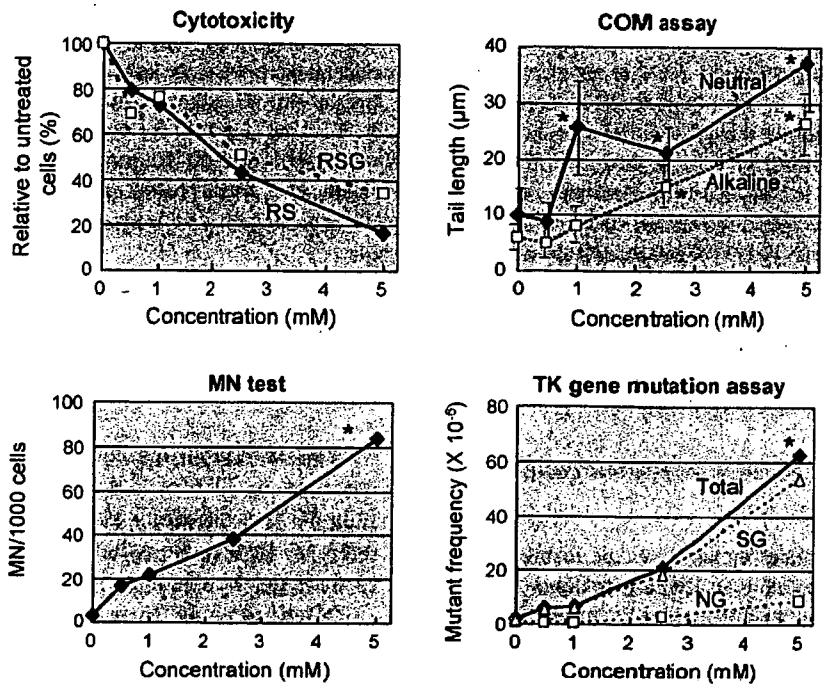

Fig. 1. Cytotoxic (relative survival, RS; relative suspension growth, RSG) and genotoxic responses (COM assay, MN test, and *TK* gene mutation assay) of TK6 cells treated with $KBrO_3$ for 4 h. Asterisk (*) statistically significant in Dunnett's test ($P < 0.05$) in COM assay, and in both pair-wise comparison and trend test ($P < 0.05$) in MN test and *TK* gene mutation assay.

mutations. Table 1 also shows the results of LOH analysis of the induced and spontaneously occurring mutants. The result of molecular analysis of spontaneous *TK* mutants was reported previously [21]. We classified the mutants into three types: non-LOH, hemizygous LOH (hemi-LOH), and homozygous LOH (homo-LOH). In general, hemi-LOH is resulted by deletion and homo-LOH is by inter-allelic homologous recombination [20]. Among the $KBrO_3$-induced mutants, 63% of NG mutants and 84% of SG mutants were hemi-LOH. In spontaneous mutants, on the other hand, majority of NG and SG mutants were non-LOH and homo-LOH, respectively. These results indicated that $KBrO_3$ predominantly induced large deletions. We previously reported the mutational spectra of *TK* mutants in TK6 cells that treated with the alkylating agent ethylmethane sulfonate (EMS), or X-irradiated [20,21]. Fig. 2 shows the comparison of the mutational spectra of spontaneous and induced *TK* mutants by EMS, X-irradiation, and $KBrO_3$. The mutation spectrum induced by $KBrO_3$ was similar to that induced by X-radiation (which also induces LOH, predominantly via deletion [21]) but not by EMS. The majority of the mutations induced by $KBrO_3$ were large deletions, but not point mutations.

Fig. 3 shows the regions of LOH and the distribution of spontaneous, X-ray-induced, and $KBrO_3$-induced

Table 1
Cytotoxic and mutational responses to $KBrO_3$, and the results of LOH analysis of normally growing (NG) and slowly growing (SG) *TK* mutants

Treatment	Cytotoxic and mutational response			LOH analysis at *TK* gene (%)			
	RSG (%)	MF ($\times 10^{-6}$)	% SG	Number	Non-LOH	Hemi-LOH	Homo-LOH
Spontaneous[a]	100	2.19	56	56			
NG mutants				19	14 (74)	3 (16)	2 (11)
SG mutants				37	0 (0)	9 (24)	28 (76)
$KBrO_3$ (2.5 mM)	51	29.4	74	39			
NG mutants				8	3 (37)	5 (63)	0 (0)
SG mutants				31	1 (3)	27 (84)	4 (13)

[a] Data from Zhan et al. [22].

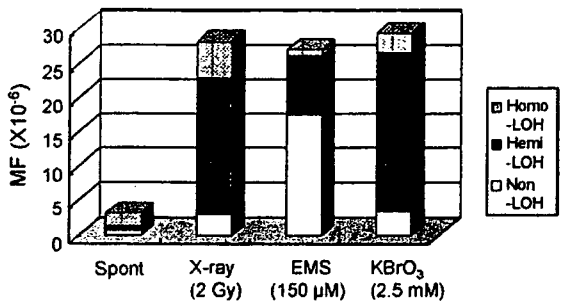

Fig. 2. *TK* mutation spectra in untreated, X-ray-treated (2 Gy), EMS-treated (150 μM, 4 h), and $KBrO_3$-treated (2.5 mM, 4 h) TK6 cells. The fraction of each mutational event was calculated by considering the ratio of NG to SG mutants and the results of molecular analysis (Table 1). The data for all but the $KBrO_3$ treatments were taken from our previous paper [20].

LOH mutants. $KBrO_3$ predominantly induced hemi-LOH, the result of large interstitial and terminal deletions, which we also frequently observed in the X-ray-induced LOH mutants. These results indicate that the genetic changes induced by $KBrO_3$ were similar to those induced by X-rays.

3.3. Gene expression analysis

Table 2 lists the genes that significantly increased expression following exposure to 2.5 mM $KBrO_3$. These genes are involved in stress response (6 genes), cell growth and DNA repair (19 genes), immune response (3 genes), apoptosis (3 genes), signal transduction (10 genes), transcription regulation (10 genes), chromosome organization (2 genes), protein modification (7 genes), energy metabolism (6 genes), lipid metabolism (2 genes), purine biosynthesis (3 genes), and unclassified functions (42 genes). Table 3 shows the genes whose expression was suppressed by the treatment. The number of up-regulated genes was greater that the number of down-regulated genes.

4. Discussion

$KBrO_3$ is a complete carcinogen, possessing both initiating and promoting activities in rodents [1]. While it shows clear positive responses in the COM assay, MN test, and chromosome aberration test using mammalian cells [4,14,17], the mutagenic potential of $KBrO_3$ in bacteria and the *Hprt* assay in Chinese hamster cells is weak or negative [1,14,17,30]. In our present study, $KBrO_3$ treatment strongly induced *TK* gene mutations. The reason we observed the induction of gene mutations and others did not is that $KBrO_3$ induces detectable mutagenecity in the *TK* gene but are only weakly mutagenic or non-mutagenic in the *Hprt* gene and in microbial assays [20]. The lower mutation frequency in the *Hprt* gene is due to the low recovery of large deletions, which are not detected because they are lethal. $KBrO_3$ is positive in mouse lymphoma cell assays that target the *Tk* gene [5]. In in vivo genotoxicity tests, $KBrO_3$ strongly induces MN in male ddY mice but is only weakly mutagenic in the *gpt* mutation assay in transgenic mice, which mainly detects point mutations and small deletions [31]. These results indicate that the property of genotoxicity

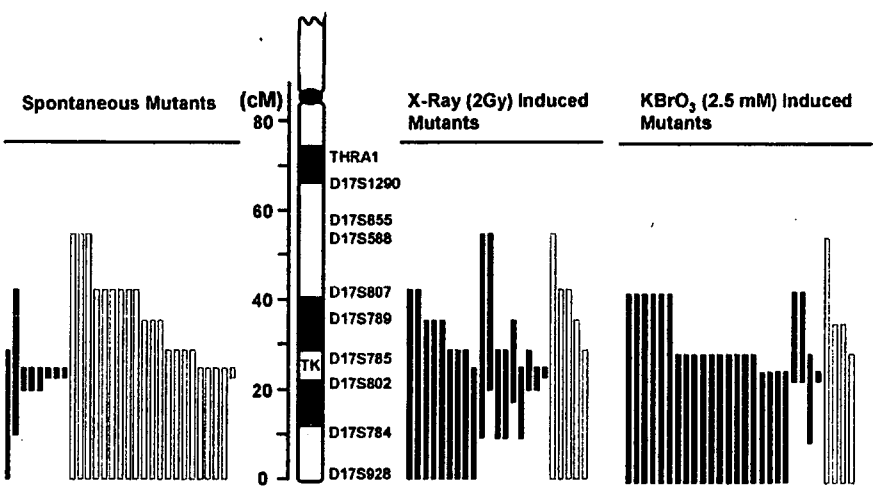

Fig. 3. The extent of LOH at the *TK* locus of TK6 cells that were untreated, X-ray-irradiated (2 Gy), or exposed to $KBrO_3$ (2.5 mM, 4 h). We examined 10 microsatellite loci on chromosome 17q that are heterozygous in TK6 cells. The human *TK* locus maps to 17q23.2. Open and closed bars represent homozygous LOH and hemizygous LOH, respectively. The length of the bar indicates the extent of the LOH. We analyzed 28 LOH mutants (4 NG and 24 SG). The data on spontaneous and X-ray-induced mutants were taken from our previous paper [20].

Table 2
Genes whose expression was up-regulated by $KBrO_3$ (2.5 mM, 4 h)

	Gene symbol	Ratio	Gene title
Stress response	CAT	2.77	Catalase
	DNAJC7	2.33	DnaJ (Hsp40) homolog, subfamily C, member 7
	FKBP5	2.87	FK506 binding protein 5
	HSPA8	3.02	Heat shock 70 kDa protein 8
	HSPCB	3.21	Heat shock 90 kDa protein 1, beta
	HSPD1	1.83	Heat shock 60 kDa protein 1
DNA repair, cell cycle, cell growth	BUB1	4.51	BUB1 budding uninhibited by benzimidazoles 1 homolog
	CCND2	5.08	Cyclin d2
	CCT2	3.33	Chaperonin containing TCP1, subunit 2 (beta)
	DKC1	2.37	Dyskeratosis congenita 1, dyskerin
	ENO1	2.10	Enolase 1 (alpha)
	HMGB1	2.16	High-mobility group box 1
	MAPRE1	2.32	Microtubule-associated protein, RP/EB family, member 1
	NME1	2.00	Non-metastatic cells 1, protein (NM23A) expressed in
	NOLC1	2.99	Nucleolar and coiled-body phosphoprotein 1
	NRAS	2.54	Neuroblastoma RAS viral (v-ras) oncogene homolog
	p21	3.22	Cyclin-dependent kinase inhibitor 1A (p21, Cip1)
	PPP2R1B	2.45	Protein phosphatase 2 (formerly 2A), regulatory subunit A (PR 65), beta isoform
	RAD21	2 34	RAD21 homolog
	RBBP4	2.00	Retinoblastoma binding protein 4
	RHOA	1.77	ras homolog gene family, member A
	SRPK1	2.75	SFRS protein kinase 1
	SSR1	2.66	Signal sequence receptor, alpha
Immune response	ARHGDIB	1.78	Rho GDP dissociation inhibitor (GDI) beta
	HLA-DRA	2.16	Major histocompatibility complex, class II, DR alpha
	IL2RG	2.43	Interleukin 2 receptor, gamma
Apoptosis	BCLAF1	6.42	BCL2-associated transcription factor 1
	FXR1	3.32	Fragile X mental retardation, autosomal homolog 1
	VDAC1	1.94	Voltage-dependent anion channel 1
Signal transduction	ANP32A	3.20	Acidic (leucine-rich) nuclear phosphoprotein 32 family, member A
	OGT	2.74	O-linked *N*-acetylglucosamine (GlcNAc) transferase
	PIP5K1A	4.25	Phosphatidylinositol-4-phosphate 5-kinase, type I, alpha
	PLEK	2.95	Pleckstrin
	PTPN11	2.61	Protein tyrosine phosphatase, non-receptor type 11
	SPTLC1	2.62	Serine palmitoyltransferase, long chain base subunit 1
	SRPR	2.52	Signal recognition particle receptor
Transcription regulation	CDC5L	4.37	CDC5 cell division cycle 5-like
	HNRPC	4.40	Heterogeneous nuclear ribonucleoprotein C (C1/C2)
	MED6	2.45	Mediator of RNA polymerase II transcription, subunit 6 homolog
	MED6	2.45	Mediator of RNA polymerase II transcription, subunit 6 homolog
	NO NO	2.68	Non-POU domain containing, octamer-binding
	POLR1C	2.67	Polymerase (RNA) I polypeptide C, 30 kDa
	PRPF4	2.51	PRP4 pre-mRNA processing factor 4 homolog
Chromosome organization	CBX5	2.68	Chromobox homolog 5 (HP1 alpha homolog, Drosophila)
Protein modification	CANX	2.56	Calnexin
	COPA	6.55	Coatomer protein complex, subunit alpha
	EIF2S3	2.40	Eukaryotic translation initiation factor 2, subunit 3 gamma
	EIF4B	2.86	Eukaryotic translation initiation factor 4B
	RANBP2	3.96	RAN binding protein 2
	SEC23IP	2.67	SEC23 interacting protein

Table 2 (*Continued*)

	Gene symbol	Ratio	Gene title
Energy pathway	AFURS1	2.83	ATPase family homolog up-regulated in senescence cells
	CYB5-M	2.54	Cytochrome *b5* outer mitochondrial membrane precursor
	TOMM22	3.07	Translocase of outer mitochondrial membrane 22 homolog
Lipid metabolism	HMGCS1	2.58	3-Hydroxy-3-methylglutaryl-Coenzyme A synthase 1
	SCD	2.56	Stearovl-CoA desaturase
Purine biosynthesis	ENTPD1	2.36	Ectonucleoside triphosphate diphosphohydrolase 1
	GART	2.64	Phosphoribosylglycinamide formyltransferase
	PAICS	1.79	Phosphoribosylaminoimidazole carboxylase
Unclassified	BANF1	2.77	Barrier to autointegration factor 1
	BAT1	1.95	HLA-B associated transcript 1///HLA-B associated transcript 1
	C1orf16	2.37	Chromosome 1 open reading frame 16
	CALU	2.40	Calumenin
	DAZAP2	2.57	DAZ associated protein 2
	DDX18	2.34	DEAD (Asp-Glu-Ala-Asp) box polypeptide 18
	DHX9	9.37	DEAH (Asp-Glu-Ala-His) box polypeptide 9
	EXOSC2	3.03	Exosome component 2
	FLJ10534	2.07	Hypothetical protein FLJ10534
	FLJ10719	2.42	Hypothetical protein FLJ10719
	FLJ12973	2.76	Hypothetical protein FLJ12973
	GANAB	2.07	Glucosidase, alpha; neutral AB
	HEM1	2.37	Hematopoietic protein 1
	IGHM	2.76	Anti-HIV-1 gp120 V3 loop antibody DO142-10 light chain variable region
	IGKC	3.15	Anti-rabies virus immunoglobulin rearranged kappa chain V-region
	LIN7C	3.51	lin-7 homolog C (*C. elegans*)
	LOC54499	2.31	Putative membrane protein
	M6PR	3.59	Mannose-6-phosphate receptor
	MGC8902	2.27	Hypothetical protein MGC8902/
	MOBK1B	2.67	MOB1, Mps one binder kinase activator-like 1B (yeast)
	NS	2.15	Nucleostemin
	NUSAP1	3.25	Nucleolar and spindle associated protein 1
	OK/SW-cl.56	1.85	Beta 5-tubulin
	OPRS1	2.76	Opioid receptor, sigma 1
	PEG 10	2.50	Paternally expressed 10
	PEX19	2.34	Peroxisomal biogenesis factor 19
	PGK1	2.11	Phosphoglycerate kinase 1
	RPE	2.35	Ribulose-5-phosphate-3-epimerase
	SDBCAG84	3.16	Serologically defined breast cancer antigen 84
	SMU1	2.70	smu-1 suppressor of mec-8 and unc-52 homolog (*C. elegans*)
	TAGLN2	2.03	Transgelin 2
	UBC	2.65	Ubiquitin C
	XPNPEP1	2.84	X-prolyl aminopeptidase
	YWHAE	6.39	Tyrosine 3-monooxygenase/tryptophan 5-monooxygenase activation protein, epsilon polypeptide
	YWHAZ	2.50	Tyrosine 3-monooxygenase/tryptophan 5-monooxygenase activation protein, zeta polypeptide

of $KBrO_3$ predominantly causes gross structural changes rather than small genetic changes such as point mutations.

$KBrO_3$ generates high yields of 8OHdG DNA adducts, which is a marker of oxidative DNA damage widely used as a predictor of carcinogenesis [10]. 8OHdG has been reported to be highly mutagenic in some experiments. In cell-free system, 8OHdG induced mutation by misincorporating adenine instead of cytosine [12]. Artificially incorporated 8OHdG at specific codons in a shuttle vector system efficiently induced GC > TA transversions in mammalian cells and *E. coli* [8,32,33]. In mammalian gene mutation assays in vitro and in vivo, however, the relationship between the accumulation of 8OHdG and the induction of GC > TA transversion has not been clear. Takeuchi et al.

Table 3
Genes whose expression was down-regulated by $KBrO_3$ (2.5 mM, 4 h)

	Gene symbol	Ratio	Gene title
Cell cycle, cell growth	FH	0.51	Fumarate hydratase
	MYC	0.55	v-myc myelocytomatosis viral oncogene homolog
Signal transduction	DUSP2	0.37	Dual specificityphosphatase 2
	RRBP1	0.39	Ribosome binding protein 1 homolog 180 kDa
	TBL3	0 43	Transducin (beta)-like3
Transcription regulation	CITED2	0.45	Cbp/p300-interacting transactivator, with Glu/Asp-rich carboxy-terminal domain, 2
	KIAA1196	0.43	KIAA1196 protein
	TZFP	0 39	Testis zinc finger protein
Chromosome organization	H1FX	0.14	H1 histone family member X
Protein modification	CLTB	0.43	Clathrin, light polypeptide (Lcb)
Energy pathway	FDX1	0.45	Ferredoxin 1
	QPRT	0.41	Quinolinate phosphoribosyltransferase
	SLC39A4	0.43	Solute carrier family 39 (zinc transporter), member 4
Unclassified	BTBD2	0.35	BTB (POZ) domain containing 2
	LOC339229	0.44	Hypothetical protein LOC339229
	MGRN1	0.44	Mahogunin, ring finger 1
	MRP63	0.41	Mitochondrial ribosomal protein 63
	PHLDA1	0.43	Pleckstrin homology-like domain, family A, member 1
	PTPLA	0.37	Protein tyrosine phosphatase-like (proline instead of catalytic arginine), member a
	SPATA2	0.45	Spermatogenesis associated 2

examined the mutagenicity of a hydroxyl radical generator, *N,N'*-bis (2-hydroxyperoxy-2-methoxyethyl)-1,4,5,8-naphthalene-tetra-carboxylic diimide (NP-III). Although NP-III highly produced 8OHdG upon irradiation with UV in V79 cells, the frequency of *Hprt* gene mutation was not significantly induced [34]. Molecular analysis demonstrated the no association of induction of 8OHdG with GC > TA transversion in the *Hprt* mutants [35]. 8OHdG is mainly removed by Ogg1 protein in a manor of the base excision repair (BER) pathway. Arai et al. investigated the relationship between the accumulation of oxidative DNA damage and the induction of gene mutation using *Ogg*1 deficient transgenic mice [36]. Although the 8OHdG level in kidneys of the *Ogg*1 deficient mice increase 200 times of the control level after 4 weeks' $KBrO_3$ treatment, the mutation frequency in the transgenic *gpt* gene was induced by less than 10 times of the control level. The molecular analysis revealed that the fraction of GC > TA transversions did not specifically increased. These results suggest that 8OHdG-mediated base substitutions do not mainly contribute to the mutagenic process involved in $KBrO_3$-induced carcinogenesis. Other genotoxic events must be involved in the carcinogenic process.

Our present studies strongly support this hypothesis. We demonstrated that $KBrO_3$ treatment clearly induced DNA damage in both the alkaline and neutral COM assay (Fig. 1). The alkaline COM assay is capable of detecting any DNA damages including DSB, single strand breaks (SSB), alkali-labile sites, DNA–DNA/DNA–protein cross-linking, and SSB associated with incomplete excision repair sites, while the neutral COM assay allows the detection of DSB, considered to be "biologically relevant" lesion of radiation damage [24]. $KBrO_3$ may have radio-mimic genotoxicity that yields oxidative DNA damage as well as DSB. $KBrO_3$ also induced MN formation and *TK* gene mutation significantly in TK6 cells. In the *TK* gene mutation assay, $KBrO_3$ predominantly produced SG mutants, but not NG mutants (Fig. 1c), implying that gross structural changes such as deletion and recombination are associated with the mutations. Molecular analysis of the *TK* mutants confirmed the assumption. Most of *TK* mutants showed LOH mutations, not non-LOH mutations, which are mainly point mutations. Harrington-Brock et al. also demonstrated that bromate compounds significantly induced *Tk* mutations in mouse lymphoma L5178Y cells, and almost all were LOH mutations [5]. LOH can be caused by deletions,

mitotic recombination between homologous alleles, or whole chromosome loss [20]. Molecular analysis can distinguish between them and reveal the mechanism and the characteristics of the mutants. In this study, $KBrO_3$ predominantly induced large deletions that resulted in hemizygous LOH (Table 1). The large deletions were mainly terminal deletions in the proximal region of chromosome 17q, which were rarely observed in spontaneously arising *TK* mutants (Fig. 3). The mutational spectrum and LOH pattern induced by $KBrO_3$ were similar to those induced by X-irradiation (Figs. 2 and 3) [20,21]. DSBs induced X-rays cause large deletions [19,20]. When the DSBs are repaired by the non-homologous end-joining pathway, interstitial deletions result. The broken chromosome ends can be also stabilized by the addition of new telomere sequences. Because TK6 cells have high telomerase activity [20], the result is terminal deletions. Thus, the major genotoxicity of $KBrO_3$ may be due to DSBs, but not to 8OHdG converting GC > TA transversion.

Some 8OHdG lesions can convert DSBs through the BER pathway [37]. In the initial step of BER, Ogg1 removes 8OHdG by DNA glycosylase activity and nicks the DNA backbone because of its associated lyase activity. The resulting SSB is processed by an apurinic endonuclease, which generates a single nucleotide gap. The gap is filled in by a DNA polymerase and sealed by a DNA ligase [38]. Clustered 8OHdG lesions induced by $KBrO_3$ may not be appropriately repaired by BER and cause DSB, however, because it is possible that two closely opposed 8OHdGs convert two closely opposed SSBs by BER resulting DSB [39,40]. Yang et al. developed Ogg1 over-expressing TK6 cell (TK6-hOGG1) and examined cytotoxic and mutagenic responses to gamma-irradiation [41]. They demonstrated that TK6-hOGG1 cells are more sensitive than the parental TK6 cells to cytotoxicity and mutagenicity by gamma-irradiation, and most of the induced *TK* mutants in TK6-OGG1 exhibited SG phenotype, which were probably large deletion mutants resulted by DSBs. This result clearly indicates that BER pathway contributes to convert oxidative damages to DSBs. Some clustered 8OHdG induced by $KBrO_3$ may covert to DSBs in TK6 cells, because TK6 is Ogg1 proficient cells [37].

To clarify the genotoxic characteristics of $KBrO_3$, we investigated the gene expression profile using Affymetrix GeneChip® Expression analysis. Many genes were up- or down-regulated by exposure to 2.5 mM $KBrO_3$ (Tables 2 and 3). Akerman et al. investigated the alterations of gene expression profiles in ionizing radiation-exposed TK6 cells [42]. They reported a >50% increase in expression of ATF-3 (stress response), Cyclin G (cell cycle), FAS antigen (apoptosis), GADD45 (repair and apoptosis), PCNA (repair), Rad51 (repair), and p21 (cell cycle) and a 40% decrease in expression of c-Myc (transcription factor), interferon stimulatory gene factor-3 (cell signaling), and p55CDC (cell cycle). We also observed up-regulation of p21 and down-regulation of c-Myc. Up-regulation of p21, however, is observed in TK6 cells exposed to any DNA-damaging chemical [43]. Islaih et al. also demonstrated the relationship between the gene expression profiles and the DNA damaging agents using TK6 cells [43]. They examined six chemicals including H_2O_2 and bleomycin which induce oxidative DNA damage. Although 10 genes were commonly up-regulated between H_2O_2 and bleomycin treatments, these genes except for p21 were not observed in our experiment. Thus, we could not find the similarity of gene expression profile by the treatment with $KBrO_3$ to by the treatment with ionizing radiation as well as oxidative damage inducers. Comparing gene expression profiles across platforms, laboratories, and experiments must be difficult [44]. Although it is difficult to judge from the expression analysis of the single chemical, information on genes which altered their expression gives a clue to understand the mechanism of action. Firstly, predominance of DNA repair and cell cycle related genes in up-regulated genes supports the genotoxic action of $KBrO_3$. Up-regulation of stress genes and apoptosis related genes suggests an involvement of oxidative stress. Up-regulation of catalase may be responsible for the oxidative damage by $KBrO_3$ (Table 2). Unclassified genes for alteration may have a functional relationship with genotoxic mechanism.

In conclusion, $KBrO_3$ predominantly induced large deletions at chromosomal level in human TK6 cells. The major genotoxicity leading to carcinogenesis of $KBrO_3$ may be due to DSBs rather than to 8OHdG adducts that lead to GC > TA transversions, as is commonly believed.

Acknowledgments

The TK6 cell line used in this study was a kind gift of Dr. John B. Little of the Harvard School of Public Health, Boston, MA. This study was supported by Health, Welfare, and Labor Science Research Grants (H15-chem-002, H15-food-004) in Japan.

References

[1] Y. Kurokawa, A. Maekawa, M. Takahashi, Y. Hayashi, Toxicity and carcinogenicity of potassium bromate—a new renal carcinogen, Environ. Health Perspect. 87 (1990) 309–335.

[2] Y. Kurokawa, S. Aoki, Y. Matsushima, N. Takamura, T. Imazawa, Y. Hayashi, Dose–response studies on the carcinogenicity of potassium bromate in F344 rats after long-term oral administration, J. Natl. Cancer Inst. 77 (1986) 977–982.
[3] A.B. DeAngelo, M.H. George, S.R. Kilburn, T.M. Moore, D.C. Wolf, Carcinogenicity of potassium bromate administered in the drinking water to male B6C3F1 mice and F344/N rats, Toxicol. Pathol. 26 (1998) 587–594.
[4] M. Ishidate Jr., K. Yoshikawa, Chromosome aberration tests with Chinese hamster cells in vitro with and without metabolic activation—a comparative study on mutagens and carcinogens, Arch. Toxicol. Suppl. 4 (1980) 41–44.
[5] K. Harrington-Brock, D.D. Collard, T. Chen, Bromate induces loss of heterozygosity in the thymidine kinase gene of L5178Y/Tk(±)-3.7.2C mouse lymphoma cells, Mutat. Res. 537 (2003) 21–28.
[6] M. Hayashi, T. Sofuni, M. Ishidate Jr., High-sensitivity in micronucleus induction of a mouse strain (MS), Mutat. Res. 105 (1982) 253–256.
[7] M. Hayashi, M. Kishi, T. Sofuni, M. Ishidate Jr., Micronucleus tests in mice on 39 food additives and eight miscellaneous chemicals, Food Chem. Toxicol. 26 (1988) 487–500.
[8] H. Kamiya, K. Miura, H. Ishikawa, H. Inoue, S. Nishimura, E. Ohtsuka, c-Ha-ras containing 8-hydroxyguanine at codon 12 induces point mutations at the modified and adjacent positions, Cancer Res. 52 (1992) 3483–3485.
[9] A.G. Knudson, Antioncogenes and human cancer, Proc. Natl. Acad. Sci. U.S.A. 90 (1993) 10914–10921.
[10] H. Kasai, S. Nishimura, Y. Kurokawa, Y. Hayashi, Oral administration of the renal carcinogen, potassium bromate, specifically produces 8-hydroxydeoxyguanosine in rat target organ DNA, Carcinogenesis 8 (1987) 1959–1961.
[11] K.C. Cheng, D.S. Cahill, H. Kasai, S. Nishimura, L.A. Loeb, 8-Hydroxyguanine, an abundant form of oxidative DNA damage, causes G–T and A–C substitutions, J. Biol. Chem. 267 (1992) 166–172.
[12] S. Shibutani, M. Takeshita, A.P. Grollman, Insertion of specific bases during DNA synthesis past the oxidation-damaged base 8-oxodG, Nature 349 (1991) 431–434.
[13] K. Sai, C.A. Tyson, D.W. Thomas, J.E. Dabbs, R. Hasegawa, Y. Kurokawa, Oxidative DNA damage induced by potassium bromate in isolated rat renal proximal tubules and renal nuclei, Cancer Lett. 87 (1994) 1–7.
[14] G. Speit, S. Haupter, P. Schutz, P. Kreis, Comparative evaluation of the genotoxic properties of potassium bromate and potassium superoxide in V79 Chinese hamster cells, Mutat. Res. 439 (1999) 213–221.
[15] T. Umemura, K. Sai, A. Takagi, R. Hasegawa, Y. Kurokawa, A possible role for oxidative stress in potassium bromate (KBrO3) carcinogenesis, Carcinogenesis 16 (1995) 593–597.
[16] K. Fujie, H. Shimazu, M. Matsuda, T. Sugiyama, Acute cytogenetic effects of potassium bromate on rat bone marrow cells in vivo, Mutat. Res. 206 (1988) 455–458.
[17] M. Ishidate Jr., T. Sofuni, K. Yoshikawa, M. Hayashi, T. Nohmi, M. Sawada, A. Matsuoka, Primary mutagenicity screening of food additives currently used in Japan, Food Chem. Toxicol. 22 (1984) 623–636.
[18] H.L. Liber, W.G. Thilly, Mutation assay at the thymidine kinase locus in diploid human lymphoblasts, Mutat. Res. 94 (1982) 467–485.
[19] H.L. Liber, D.W. Yandell, J.B. Little, A comparison of mutation induction at the tk and hprt loci in human lymphoblastoid cells; quantitative differences are due to an additional class of mutations at the autosomal tk locus, Mutat. Res. 216 (1989) 9–17.
[20] M. Honma, Generation of loss of heterozygosity and its dependency on p53 status in human lymphoblastoid cells, Environ. Mol. Mutagen. 45 (2005) 162–176.
[21] M. Honma, M. Hayashi, T. Sofuni, Cytotoxic and mutagenic responses to X-rays and chemical mutagens in normal and p53-mutated human lymphoblastoid cells, Mutat. Res. 374 (1997) 89–98.
[22] L. Zhan, H. Sakamoto, M. Sakuraba, D.S. Wu, L.S. Zhang, T. Suzuki, M. Hayashi, M. Honma, Genotoxicity of microcystin-LR in human lymphoblastoid TK6 cells, Mutat. Res. 557 (2004) 1–6.
[23] N. Koyama, H. Sakamoto, M. Sakuraba, T. Koizumi, Y. Takashima, M. Hayashi, H. Matsufuji, K. Yamagata, S. Masuda, N. Kinae, M. Honma, Genotoxicity of acrylamide and glycidamide in human lymphoblastoid TK6 cells, Mutat. Res. 603 (2006) 151–158.
[24] S. Wada, H. Kurahayashi, Y. Kobayashi, T. Funayama, K. Yamamoto, M. Natsuhori, N. Ito, The relationship between cellular radiosensitivity and radiation-induced DNA damage measured by the comet assay, J. Vet. Med. Sci. 65 (2003) 471–477.
[25] M. Watanabe-Akanuma, T. Ohta, Y.F. Sasaki, A novel aspect of thiabendasole as a photomutagen in bacteria and cultured human cells, Mutat. Res. 158 (2005) 213–219.
[26] T. Matsushima, M. Hayashi, A. Matsuoka, M. Ishidate Jr., K.F. Miura, H. Shimizu, Y. Suzuki, K. Morimoto, H. Ogura, K. Mure, K. Koshi, T. Sofuni, Validation study of the in vitro micronuclei test in a Chinese hamster lung cell line (CHL/IU), Mutagenesis 14 (1999) 569–580.
[27] T. Omori, M. Honma, M. Hayashi, Y. Honda, I. Yoshimura, A new statistical method for evaluating of L5178Ytk± mammalian cell data using microwell method 517 (2002) 199–208.
[28] M. Honma, M. Momose, H. Tanabe, H. Sakamoto, Y. Yu, J.B. Little, T. Sofuni, M. Hayashi, Requirement of wild-type p53 protein for maintenance of chromosomal integrity, Mol. Carcinog. 28 (2000) 203–214.
[29] P.L. Olive, DNA damage and repair in individual cells: applications of the comet assay in radiobiology, Int. J. Radiat. Biol. 75 (1999) 395–405.
[30] D.E. Levin, M. Hollstein, M.F. Christman, E.A. Schwiers, B.N. Ames, A new Salmonella tester strain (TA102) with A X T base pairs at the site of mutation detects oxidative mutagens, Proc. Natl. Acad. Sci. U.S.A. 79 (1982) 7445–7449.
[31] T. Arai, V.P. Kelly, O. Minowa, T. Noda, S. Nishimura, High accumulation of oxidative DNA damage, 8-hydroxyguanine, in Mmh/Ogg1 deficient mice by chronic oxidative stress, Carcinogenesis 23 (2002) 2005–2010.
[32] F. Le Page, A. Margot, A.P. Grollman, A. Sarasin, A. Gentil, Mutagenicity of a unique 8-oxoguanine in a human Ha-ras sequence in mammalian cells, Carcinogenesis 16 (1995) 2779–2784.
[33] M.L. Wood, M. Dizdaroglu, E. Gajewski, J.M. Essigmann, Mechanistic studies of ionizing radiation and oxidative mutagenesis: genetic effects of a single 8-hydroxyguanine (7-hydro-8-oxoguanine) residue inserted at a unique site in a viral genome, Biochemistry 29 (1990) 7024–7032.
[34] T. Takeuchi, S. Matsugo, K. Morimoto, Mutagenicity of oxidative DNA damage in Chinese hamster V79 cells, Carcinogenesis 18 (1997) 2051–2055.
[35] M. Nakajima, T. Takeuchi, K. Ogino, K. Morimoto, Lack of direct involvement of 8-hydroxy-2′-deoxyguanosine in

hypoxanthine-guanine phosphoribosyltransferase mutagenesis in V79 cells treated with *N,N'*-bis(2-hydroxyperoxy-2-methoxy-ethyl)-1,4,5,8-naphthalenetetracarboxyli c-diimide (NP-III) or riboflavin, Jpn. J. Cancer Res. 93 (2002) 247–252.

[36] T. Arai, V.P. Kelly, K. Komoro, O. Minowa, T. Noda, S. Nishimura, Cell proliferation in liver of Mmh/Ogg1-deficient mice enhances mutation frequency because of the presence of 8-hydroxyguanine in DNA, Cancer Res. 63 (2003) 4287–4292.

[37] N. Yang, M.A. Chaudhry, S.S. Wallace, Base excision repair by hNTH1 and hOGG1: a two edged sword in the processing of DNA damage in gamma-irradiated human cells, DNA Repair (Amst.) 5 (2006) 43–51.

[38] G. Slupphaug, B. Kavli, H.E. Krokan, The interacting pathways for prevention and repair of oxidative DNA damage, Mutat. Res. 531 (2003) 231–251.

[39] K. Tian, M. McTigue, S.C. de los, Sorting the consequences of ionizing radiation: processing of 8-oxoguanine/abasic site lesions, DNA Repair (Amst.) 1 (2002) 1039–1049.

[40] M.E. Lomax, S. Cunniffe, P. O'Neill, Efficiency of repair of an abasic site within DNA clustered damage sites by mammalian cell nuclear extracts, Biochemistry 43 (2004) 11017–11026.

[41] N. Yang, H. Galick, S.S. Wallace, Attempted base excision repair of ionizing radiation damage in human lymphoblastoid cells produces lethal and mutagenic double strand breaks, DNA Repair (Amst.) 3 (2004) 1323–1334.

[42] G.S. Akerman, B.A. Rosenzweig, O.E. Domon, C.A. Tsai, M.E. Bishop, L.J. McGarrity, J.T. Macgregor, F.D. Sistare, J.J. Chen, S.M. Morris, Alterations in gene expression profiles and the DNA-damage response in ionizing radiation-exposed TK6 cells, Environ. Mol. Mutagen. 45 (2005) 188–205.

[43] M. Islaih, B.W. Halstead, I.A. Kadura, B. Li, J.L. Reid-Hubbard, L. Flick, J.L. Altizer, D.J. Thom, D.K. Monteith, R.K. Newton, D.E. Watson, Relationships between genomic, cell cycle, and mutagenic responses of TK6 cells exposed to DNA damaging chemicals, Mutat. Res. 578 (2005) 100–116.

[44] C.L. Yauk, M.L. Berndt, A. Williams, G.R. Douglas, Comprehensive comparison of six microarray technologies, Nucleic Acids Res. 32 (2004) e124.

THE JOURNAL OF BIOLOGICAL CHEMISTRY VOL. 282, NO. 46, pp. 33507–33514, November 16, 2007

A New Role of Thrombopoietin Enhancing *ex Vivo* Expansion of Endothelial Precursor Cells Derived from AC133-positive Cells*

Received for publication, May 14, 2007, and in revised form, September 5, 2007 Published, JBC Papers in Press, September 7, 2007, DOI 10.1074/jbc.M703919200

Toshie Kanayasu-Toyoda[‡], Akiko Ishii-Watabe[‡], Takayoshi Suzuki[§], Tadashi Oshizawa[§], and Teruhide Yamaguchi[‡1]

From the Divisions of [‡]Biological Chemistry and Biologicals, and [§]Cellular and Gene Therapy Products, National Institute of Health Sciences, Kamiyoga 1-18-1, Setagayaku, Tokyo 158-8501, Japan

We previously reported that CD31^{bright} cells, which were sorted from cultured AC133$^+$ cells of adult peripheral blood cells, differentiated more efficiently into endothelial cells than CD31$^+$ cells or CD31$^-$ cells, suggesting that CD31^{bright} cells may be endothelial precursor cells. In this study, we found that CD31^{bright} cells have a strong ability to release cytokines. The mixture of vascular endothelial growth factor (VEGF), thrombopoietin (TPO), and stem cell factor stimulated *ex vivo* expansion of the total cell number from cultured AC133$^+$ cells of adult peripheral blood cells and cord blood cells, resulting in incrementation of the adhesion cells, in which endothelial nitric oxide synthase and kinase insert domain-containing receptor were positive. Moreover, the mixture of VEGF and TPO increased the CD31^{bright} cell population when compared with VEGF alone or the mixture of VEGF and stem cell factor. These data suggest that TPO is an important growth factor that can promote endothelial precursor cells expansion *ex vivo*.

Neovascularization is an important adaptation to rescue tissue from critical ischemia. Postnatal blood vessel formation was formerly thought to be primarily due to the migration and proliferation of preexisting, fully differentiated endothelial cells, a process referred to as angiogenesis. Recent studies provide increasing evidence that circulating bone marrow-derived endothelial progenitor cells (EPCs)[2] contribute substantially to adult blood vessel formation (1–5). Cell therapy using EPCs is widely performed to rescue tissue damaged due to critical ischemia.

Although EPCs have been thought to be derived from many kinds of cells, cells characterized as CD34$^+$ (6), AC133$^+$ (7, 8), and CD14$^+$ (9) are also thought to differentiate to EPCs. The main role of EPCs has been thought to be the release of angiogenic factors such as interleukin-8 (IL-8), granulocyte colony-stimulating factor (G-CSF), hepatocyte growth factor, and vascular endothelial growth factor (VEGF) (9). To obtain a sufficient number of EPCs for the treatment may be very important in cell therapy for critical ischemia.

On the other hand, EPCs are mobilized from bone marrow by many substances such as G-CSF (10), granulocyte macrophage-colony stimulating factor (GM-CSF) (5), VEGF (3), erythropoietin (11–13), and statins (14, 15) *in vivo*. To get as many EPCs as possible without unduly burdening the patient, it is desirable to establish efficient expansion methods for EPCs *in vitro*.

Thrombopoietin (TPO), initially identified as the primary regulator of platelet production (16), plays an important and nonredundant role in the self-renewal of and expansion methods for hematopoietic stem cells (17–19). Recently, TPO has been found to exert a proangiogenic effect on cultured endothelial cells (20). The mechanism by which hematopoietic cytokines support revascularization *in vivo*, however, remains unknown. TPO has increased the number of colony-forming units-granulocyte-macrophage (21) and of burst-forming units-erythroid (22) *in vivo* and leads to a redistribution of colony-forming units-erythroid from marrow to spleen. Moreover, TPO acts in synergy with erythropoietin to increase the growth of burst-forming units-erythroid and the generation of colony-forming units-erythroid from marrow cells (21, 23, 24).

In our previous study (25), we isolated AC133$^+$ cells and examined their endothelial differentiation *in vitro*. CD31(PECAM-1)$^+$ and CD31^{bright} cells appeared at an early stage of the *in vitro* differentiation of AC133$^+$ cells, and CD31^{bright} cells derived from AC133$^+$ cells were identified as the precursors of endothelial cells because CD31^{bright} cells had differentiated more efficiently to endothelial cells than others. Therefore, we conclude that CD31^{bright} cells derived from AC133$^+$ cells possess the typical character of EPCs. In this study, we analyzed the effects of TPO on the appearance of CD31^{bright} cells from AC133$^+$ cells, and we show that TPO plays an important role in *in vitro* EPC expansion.

EXPERIMENTAL PROCEDURES

Reagents—Recombinant TPO and recombinant stem cell factor (SCF) were kindly provided by Kirin-Amgen Inc. (Thousand Oaks, CA). Recombinant human VEGF was purchased from Strathmann Biotec AG (Hamburg, Germany). The AC133

* This work was supported in part by a grant-in-aid for health and labor science research from the Japanese Ministry of Health, Labor, and Welfare, and in part by a grant-in-aid for Research on Health Sciences focusing on Drug Innovation from the Japan Health Sciences Foundation. The costs of publication of this article were defrayed in part by the payment of page charges. This article must therefore be hereby marked "*advertisement*" in accordance with 18 U.S.C. Section 1734 solely to indicate this fact.

[1] To whom correspondence should be addressed. Tel.: 81-3-3700-9064; Fax: 81-3-3707-6950; E-mail: yamaguch@nihs.go.jp.

[2] The abbreviations used are: EPCs, endothelial precursor cells; VEGF, vascular endothelial growth factor; FN, fibronectin; PBS, phosphate-buffered saline; FITC, fluorescein isothiocyanate; PE, phycoerythrin; TPO, thrombopoietin; SCF, stem cell factor; G-CSF, granulocyte colony-stimulating factor; GM-CSF, granulocyte macrophage-colony stimulating factor; IL, interleukin; PI3K, phosphatidylinositol 3-kinase; VEcad, vascular endothelial cadherin; eNOS, endothelial nitric oxide synthase; FBS, fetal bovine serum; STAT, signal transducers and activators of transcription; JAK, Janus kinase; KDR, kinase insert domain-containing receptor.

magnetic cell sorting kit and phycoerythrin (PE)-conjugated anti-CD133/2 antibody were from Miltenyi Biotec (Gladbach, Germany). Allophycocyanin-conjugated anti-CD110 (TPO receptor) antibody, fluorescein isothiocyanate (FITC)-conjugated anti-CD31 monoclonal antibody, FITC-conjugated anti-CD34 monoclonal antibody, and anti-STAT3 monoclonal antibody were from Pharmingen. Phycoerythrin-conjugated vascular endothelial cadherin (VEcad/CD144) antibody was from Beckman Coulter (Marseilles, France). Anti-vascular endothelial growth factor receptor-2 (Flk-1/KDR) monoclonal antibody (Santa Cruz Biotechnology, Inc., Santa Cruz, CA) and anti-human endothelial nitric oxide synthase (eNOS) rabbit polyclonal antibody (Cayman Chemical, Ann Arbor, MI) were obtained. Anti-phospho-Akt (Ser-473) antibody, anti-Akt antibody, and anti-phospho-STAT3 (Tyr-705) antibody were from Cell Signaling Technology (Beverly, MA). Fibronectin (FN)- and type IV collagen-coated dishes were purchased from Iwaki Co., Tokyo, Japan. Phycoerythrin-conjugated anti-CD14 antibody was from DakoCytomation (Glostrup, Denmark).

Preparation of Peripheral Blood Mononuclear Cells—Human cord blood was kindly supplied by the Metro Tokyo Red Cross Cord Blood Bank (Tokyo, Japan) with informed consent. The buffy coat fraction was prepared from voluntary donated human blood of Saitama Red Cross of Japan (Saitama, Japan). The blood sample was diluted with phosphate-buffered saline (PBS) containing 2 mM EDTA and was loaded on a Lymphoprep™ tube (Axis-Shield PoC AS, Oslo Norway) (density = 1.077). After being centrifuged for 20 min 800 × *g* at 18 °C, mononuclear cells were collected and washed with sorting solution (PBS supplemented with 2 mM EDTA and 0.5% bovine serum albumin).

Flow Cytometric Analysis of AC133 and CD34 Expression in Mononuclear Cells—To eliminate the dead cells, dead cells were stained with 7-amino actinomycin D. Mononuclear cells were labeled with PE-conjugated anti-AC133 monoclonal antibody and FITC-conjugated anti-CD34 monoclonal antibody simultaneously at 4 °C for 30 min. After washing with the sorting solution, flow cytometric analysis was performed with a FACSCalibur (BD Biosciences).

Magnetic Cell Sorting of $AC133^+$ Cells—Mononuclear cells were labeled with magnetic bead-conjugated anti-AC133 antibodies according to the protocol directed by the manufacturer. After the brief wash with the sorting solution, the cells were separated by a magnetic cell separator (autoMACS, Miltenyi Biotec, Gladbach, Germany), and the positive cells were then collected.

Culture of $AC133^+$ Cells—Isolated $AC133^+$ cells were cultured in EBM-2 (Cambrex Corp., East Rutherford, NJ) medium containing 20% heat-inactivated FBS and 30 mg/liter kanamycin sulfate at 37 °C under moisturized air containing 5% CO_2 with 50 ng/ml VEGF as control medium. Control medium containing VEGF was added with TPO, SCF, or both. Cells were plated on FN- or type IV collagen-coated dishes at a cell density of $\sim 10^6$ cells/ml. We have previously shown that EPCs can tightly adhere to an FN-coated dish but weakly to type IV collagen-coated dish (25). Analysis of adherent EPCs was performed on FN-coated dish and that of suspended EPCs on type IV collagen-coated dish. Half of the medium was exchanged once every 3–4 days with fresh medium. Adherent cells on FN-coated dish were fixed with ethanol chilled to −20 °C and then subsequently subjected to an immunostaining procedure or other treatments. Cells on type IV collagen-coated dish were subsequently subjected to flow cytometric analysis.

Immunostaining of Adherent Cells—After fixation with chilled ethanol (−20 °C), the cell layer was washed three times with PBS. Cells were incubated with 1% bovine serum albumin in PBS (−) for 1 h at 4 °C for blocking and then with each first antibody in 1% bovine serum albumin in PBS (−) for 1 h at 4 °C. After washing with PBS, the cells were incubated with FITC-conjugated anti-mouse IgG antibody or rhodamine-conjugated anti-rabbit IgG antibody for 1 h at 4 °C. Cells were washed with PBS and then examined using a Zeiss LSM 510 microscope with an excitation wavelength of 488 nm and an emission of 530/30 nm for FITC or 570/30 nm for rhodamine.

In every experiment, we used nonspecific immunoglobulin corresponding to the first antibody species as a control and confirmed that the cells were not stained with control immunoglobulin. The fluorescence intensity of 20 randomly selected cells was calculated using the Scion Image program within the linear range for quantitation.

Analysis of Cytokines in the Supernatant of $CD31^{bright}$ and $CD31^+$ Cells—The expression of CD31 on cultured $AC133^+$ cells was determined with a flow cytometer. After $AC133^+$ cells were cultured for several days on either FN-coated or collagen type IV-coated dishes, both adherent and nonadherent cells were collected. The collected cells were labeled with FITC-labeled anti-CD31 antibody for 15 min at 4 °C. After a brief wash with 0.5% bovine serum albumin in PBS, flow cytometric analysis was performed. $CD31^{bright}$ and $CD31^+$ cells were sorted from cultured $AC133^+$ cells with FACSAria (BD Biosciences). Sorted cells of both populations were subsequently cultured in EBM-2 supplemented with 20% FBS in the absence of any cytokines. After 5 days, the collected supernatant of cells was frozen at −20 °C. Cytokines were measured by a BD™ cytometric beads array Flex set system (BD Biosciences) according to the manufacturer's protocol.

Flow Cytometric Analysis of Various Cell Surface Markers in Cultured $AC133^+$ Cells—After $AC133^+$ cells were cultured for the indicated period, cells were co-stained with FITC-labeled anti-CD31 antibody and PE-labeled anti-CD14 antibody or PE-labeled VEcad antibody. Cells were also stained with FITC-labeled anti-CD31 antibody, allophycocyanin-labeled anti-CD110 antibody, and PE-labeled anti-AC133 antibody triply and then subjected to flow cytometry. Dead cells were eliminated by staining with 7-amino actinomycin D.

Calculation of the Absolute Number of $CD31^{bright}$ Cells—The absolute number of $CD31^{bright}$ cells was multiplied by the total cell number of each well, and the ratio of $CD31^{bright}$ cells was analyzed by fluorescence-activated cell sorter.

Preparation of Cell Lysates and Immunoblotting—After cell sorting, $AC133^+$ cells were suspended in 20% FBS-EBM2 and cultured for 3 days in the presence of VEGF and TPO. Cells were collected and incubated in 2% FBS-EBM2 for 1 h. Cells were stimulated by 50 ng/ml TPO, 50 ng/ml VEGF, or both for 15 min. Cells (1×10^6) were collected and lysed in lysis buffer containing 1% Triton X-100, 10 mM K_2HPO_4/KH_2PO_4 (pH

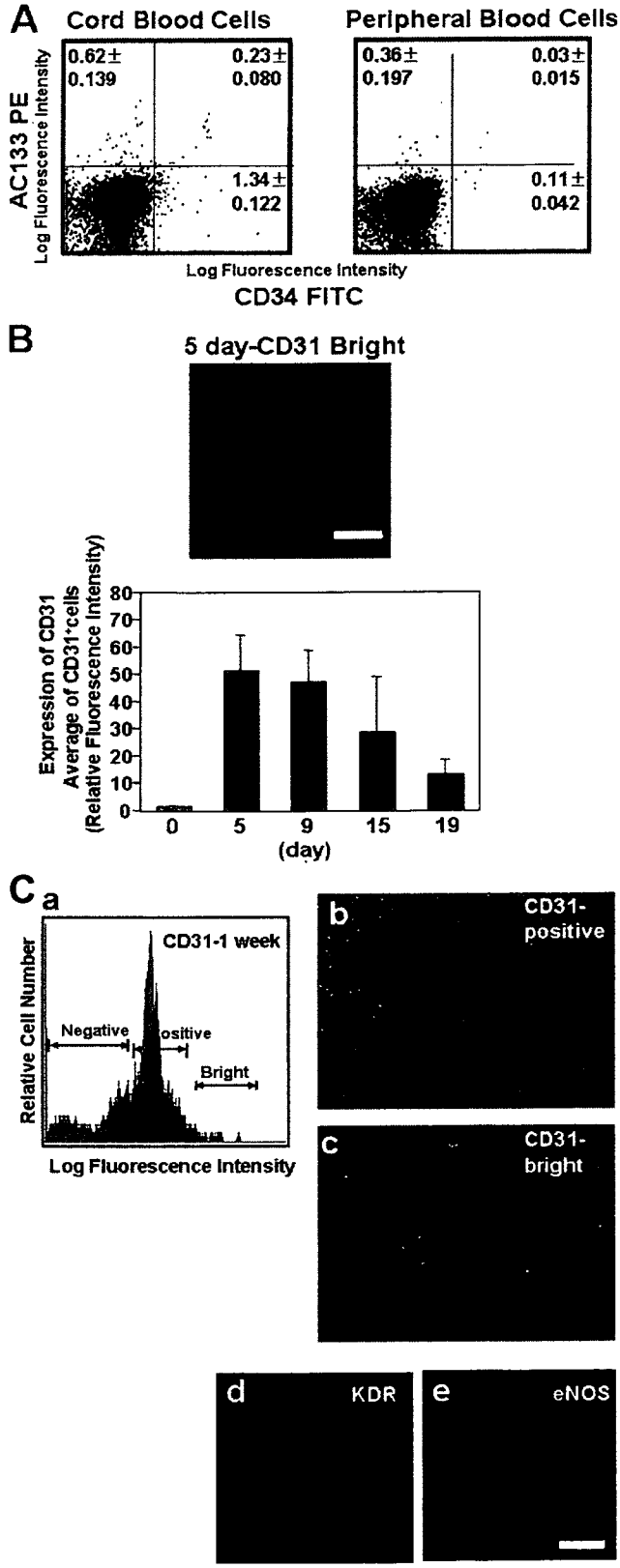

FIGURE 1. ***In vitro* differentiation of AC133$^+$ cells of cord blood into endothelial cells.** *A*, expression of AC133 and CD34 cells in human cord blood and peripheral blood mononuclear cells was analyzed by staining with AC133-PE (*vertical axis*) and CD34-FITC (*horizontal axis*). The *numbers* in the flow cytometric dot blots indicates the percentage of each population ± S.D. *B*, when AC133$^+$ cells were cultured for 19 days in the presence of VEGF on FN-coated dishes, the appearance of CD31$^+$ cells was analyzed. The *upper panel* shows the fluorescent photomicrograph of adhesion cells stained with FITC-conjugated anti-CD31 antibody after a 5-day culture. Quantitation of the fluorescence intensity of 20 CD31-positive cells was analyzed as described under "Experimental Procedures." Columns and bars represent the means ± S.D. from 20 cells (*B, lower panel*). *C*, the CD31-negative, positive, and bright cell populations prepared after 1-week cultivation of AC133$^+$ cells are shown in a representative histogram stained with FITC-conjugated anti-CD31 antibody. The *x* axis represents the log fluorescence intensity of CD31-FITC, *y* axis relative cell number (*panel a*). *Panels b* and *c* show phase-contrast microscopic photographs of cultured CD31-positive and bright cells, respectively, subsequently cultured for 1 week after cell sorting. The *bottom panels d* and *e* show the fluorescent photomicrographs of adhesion cells from the CD31^{bright} fraction stained with anti-KDR antibody and anti-eNOS antibody, respectively. *Scale bar*, 100 μm.

7.5), 1 mM EDTA, 5 mM EGTA, 10 mM $MgCl_2$, and 50 mM β-glycerophosphate, along with 1/100 (v/v) protease inhibitor mixture (Sigma) and 1/100 (v/v) phosphatase inhibitor mixture (Sigma). The cellular lysate of 5 × 10^5 cells/lane was subjected to Western blotting analysis.

Statistical Analysis—Statistical analysis was performed using the unpaired Student's *t* test, and the dose response of TPO was compared between the four groups by one-way analysis of variance and the Tukey test using Prism 4 software. Values of $p < 0.05$ were considered to indicate statistical significance. Each experiment was repeated three times, and the representative data are indicated.

RESULTS

We previously reported that during the *in vitro* differentiation of peripheral blood AC133$^+$ cells into the endothelial cells, the expression of CD31 was the earliest marker among all of the tested markers (25). Moreover, by analyzing the ability of differentiation into endothelial cells, CD31^{bright} cells were shown to exhibit EPC character when compared with the CD31$^+$ fraction. Since cord blood is a rich source of blood stem cells such as CD34$^+$ and AC133$^+$ cells, it is expected to be a useful source for CD31^{bright} cells. At first, we attempted to determine whether the CD31^{bright} fraction derived from cord blood AC133$^+$ cells contained EPCs. As shown in Fig. 1*A*, the populations of AC133$^+$ CD34$^-$ cells, AC133$^-$ CD34$^+$ cells, and AC133$^+$ CD34$^+$ cells in cord blood were approximately four times greater than those in peripheral blood (Fig. 1*A*). After 5 days of cultivation of AC133$^+$ cells on an FN-coated dish, adherent CD31-positive cells were observed (Fig. 1*B*, *upper panel*). Analysis of the fluorescence intensity of CD31-positive cells revealed that the average fluorescence intensity in CD31$^+$ cells was highest on day 5 (Fig. 1*B*, *lower panel*), corresponding to the results of peripheral blood cells.

After 1 week of cultivation of AC133$^+$ cells on a collagen type IV-coated dish, on which cells adhered more loosely when compared with the FN-coated dish, cells were collected and sorted into CD31$^+$ and CD31^{bright} fractions, as shown in Fig. 1*C*, *panel a*, and both cell types were cultured on an FN-coated dish for 1 week after the sorting. The number of cells adhering and spreading was higher in the CD31^{bright} fraction (Fig. 1*C*, *panel c*) than in the CD31$^+$ fraction (Fig. 1*C*, *panel b*), and these adhering cells are apparently KDR- (Fig. 1*C*, *panel d*) and eNOS-positive (Fig. 1*C*, *panel e*). The large areas of intense green fluorescence represent the colonies of CD31^{bright} cells. These data indicate that CD31^{bright} cells derived from AC133$^+$ cells of both peripheral blood and cord blood are EPCs.

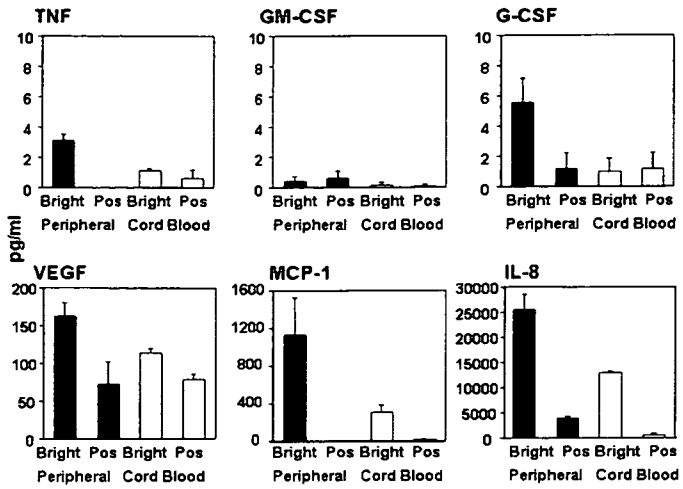

FIGURE 2. **Various cytokines released from CD31$^+$ cells and CD31^{bright} cells.** Production of various cytokines from CD31$^+$ cells and CD31^{bright} cells derived from AC133$^+$ cells cultivated for 5 days was measured. *Gray columns* indicate the cytokine production by cells from peripheral blood and open columns from cord blood. Columns and bars represent the means ± S.D. from three separate experiments. *TNF*, tumor necrosis factor; *Pos*, positive; *MCP-1*, monocyte chemoattractant protein-1.

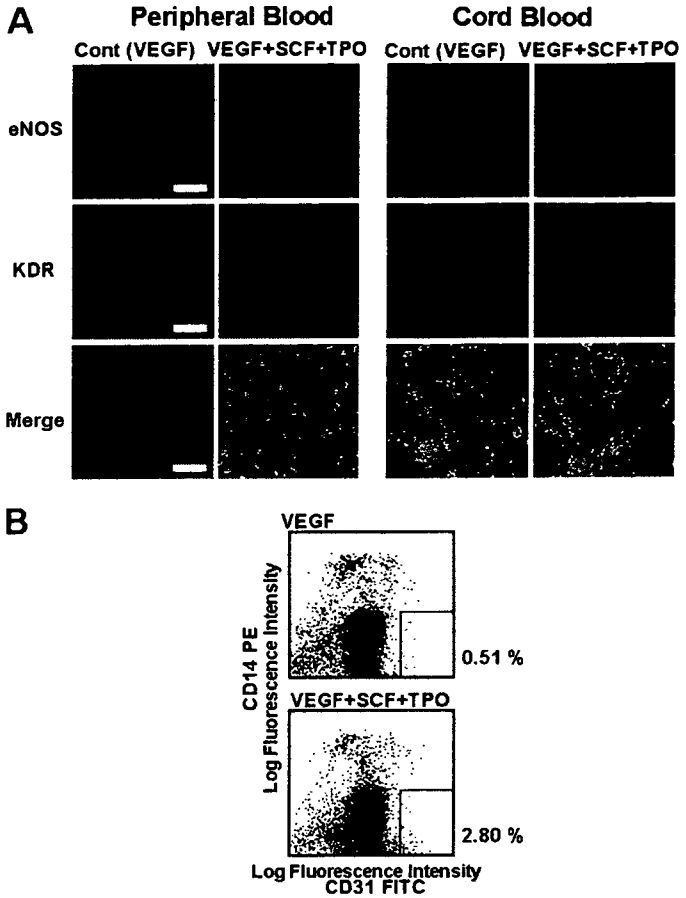

FIGURE 3. **Increment of EPCs from AC133$^+$ cells in the presence of TPO and SCF.** *A*, AC133$^+$ cells were differentiated for 2 weeks in the presence of either VEGF alone or the combination of TPO, SCF, and VEGF on an FN-coated dish. The *upper* and *middle panels* indicate the fluorescent photomicrographs of cells stained with anti-eNOS antibody and anti-KDR antibody, respectively. The *bottom panels* indicate the merged images of both antibodies. From the *left side*, control (*Cont*) and the mixture of peripheral blood, control, and the mixture of cord blood. *Scale bar*, 100 μm. *B*, CD14 and CD31 expression in cultured AC133$^+$ cells for 1 week was stained with CD14-PE (*vertical axis*) and CD31-FITC (*horizontal axis*). The *upper panel* indicates cells treated with VEGF alone, and the *lower panel* indicates cells treated with the mixture of VEGF, SCF, and TPO. The *number* on the *right side* of the flow cytometric dot blot indicates the percentage of the CD14$^-$ CD31^{bright} population.

Several reports have shown that EPCs produce cytokines (9, 26, 27), but the ability of CD31$^+$ or CD31^{bright} cells derived from AC133$^+$ cells to produce cytokines is not known. After cell sorting, quantitative analysis of cytokines released by CD31$^+$ cells and CD31^{bright} cells was carried out at 5 days after the cultivation. As shown in Fig. 2, IL-8 was markedly produced by CD31^{bright} cells from both peripheral blood and cord blood when compared with CD31$^+$ cells. The production of monocyte chemoattractant protein-1 (MCP-1) by CD31^{bright} cells was also higher than that of CD31$^+$ cells. The production of VEGF was higher by CD31^{bright} cells than by CD31$^+$ cells but not significantly. The production of all cytokines by CD31^{bright} cells from peripheral blood was higher than that from cord blood. Tumor necrosis factor-α, GM-CSF, and G-CSF were hardly produced by CD31^{bright} and CD31$^+$ cells. These data indicate that CD31^{bright} cells derived from AC133$^+$ cells have a strong ability to produce chemokines.

It has been reported that TPO and SCF are potent stimulators of multipotent cell proliferation (17, 19). Next, the effects of both growth factors on EPC growth and differentiation in our culture system were determined. After the addition of both TPO and SCF for 2 weeks, the expression of eNOS and KDR in adhered cells was analyzed (Fig. 3*A*). Fig. 3*A* clearly indicates that AC133$^+$ cells from both peripheral blood and cord blood differentiate into eNOS$^+$ and KDR$^+$ cells more efficiently in the presence of the mixture of TPO, SCF, and VEGF than of VEGF alone. Flow cytometric analysis revealed that the ratio of CD31^{bright} CD14$^-$ cells increased in the presence of the mixture of TPO, SCF, and VEGF when AC133$^+$ cells were cultured on collagen type IV-coated dish for 1 week (Fig. 3*B*).

We next examined which growth factor is dominant in the induction and proliferation of CD31^{bright} cells. The total cell number of cultured AC133$^+$ cells from both peripheral blood (Fig. 4*A*, *upper panel*) and cord blood (Fig. 4*A*, *lower panel*) significantly increased in the presence of TPO, SCF, or both growth factors when compared with that of VEGF alone during a 1-week period. As shown in Fig. 4*B*, however, the increment in the ratio of the CD31^{bright} cell population was observed only in the presence of TPO. The absolute number of CD31^{bright} cells, calculated by the total cell number and the ratio of the CD31^{bright} cell population, was markedly increased by TPO (Fig. 4*C*). In contrast, SCF induced the increase in total cell number to the same level as TPO (Fig. 4*A*), but it did not induce the increase in either the ratio of the CD31^{bright} cell population (Fig. 4*B*) or the number of CD31^{bright} cells (Fig. 4*C*). Next, we examined whether TPO and VEGF can synergistically affect the induction of CD31^{bright} cells during a 1-week cultivation. As shown in Fig. 4*D*, although VEGF had no effects on the total cell number (Fig. 4*D*, *panel a*), it increased the ratio of the CD31^{bright} cell population to 1.4-fold higher than that of the control (Fig. 4*D*, *panel b*), resulting in a slight increase in the number of CD31^{bright} cells (Fig. 4*D*, *panel c*). Thrombopoietin alone induced an increase in not only the total cell number (Fig. 4*D*, *panel a*) but also the ratio of the CD31^{bright} cell population (Fig. 4*D*, *panel b*), resulting in an ~24-fold increment of the absolute

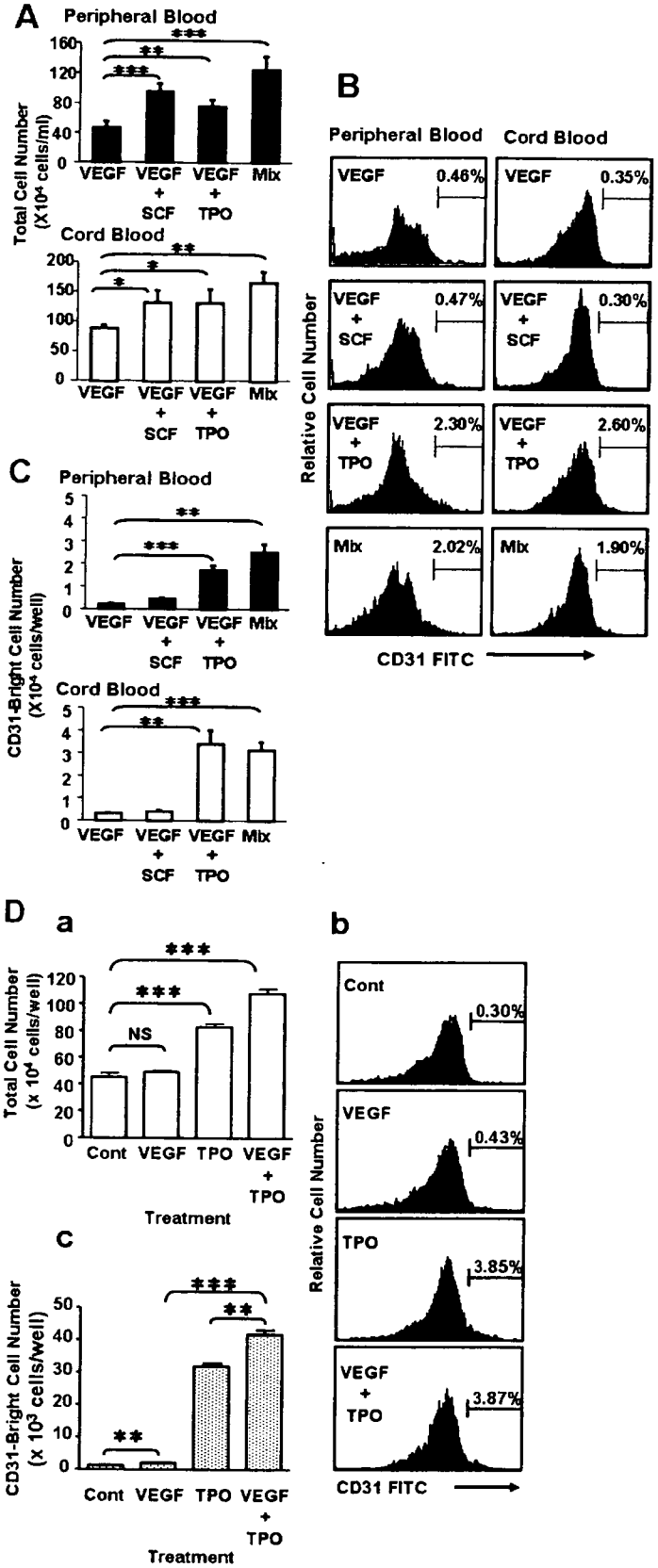

FIGURE 4. **Stimulative effects of TPO on induction of CD31^{bright} cells.** *A*, alteration of the cell number of cultivated AC133$^+$ cells for 1 week in the combination of growth factors. *Mix*, VEGF + SCF + TPO. *B*, the flow cytometric histogram of AC133$^+$-derived cells stained with FITC-labeled anti-CD31 antibody after a 1-week culture. The *representing number* in the flow cytometric histogram indicates the percentage of the CD31^{bright} cell population. The *left panels* are peripheral blood, and the *right panels* are cord blood. *C*, CD31^{bright} cells numbers were calculated by both the total cell number and the ratio the of CD31^{bright} population. *D*, the effects of TPO alone on EPC differentiation derived from AC133$^+$ cells of cord blood. The *upper left panel* (*a*) shows the total cell number after a 1-week culture, the *right panels* (*b*) show the flow cytometric histogram of AC133$^+$-derived cells stained with FITC-labeled anti-CD31 antibody, and the *lower left panel* (*c*) shows the calculated CD31^{bright} cell number. Columns and bars represent the means ± S.D. (*, $p < 0.05$; **, $p < 0.01$; ***, $p < 0.001$). *NS*, not significant; *Cont*, control.

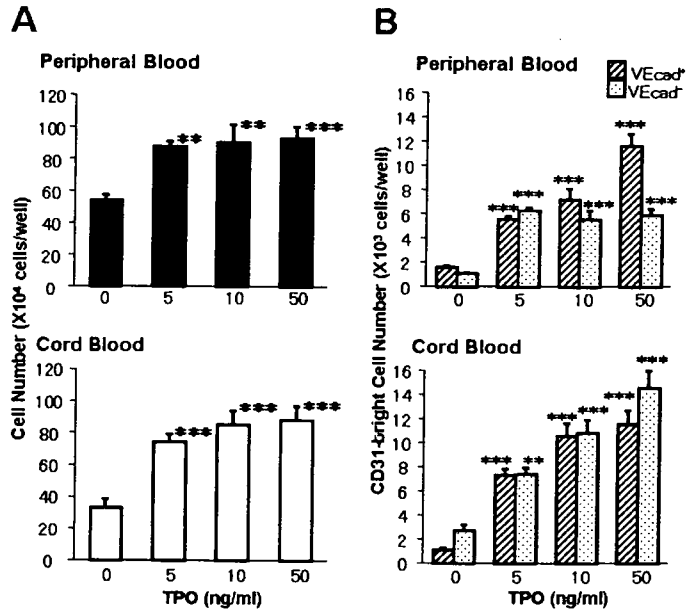

FIGURE 5. **Dose-dependent effects of TPO on the induction of CD31^{bright} cells from AC133$^+$ cells.** AC133$^+$ cells were treated with various concentrations of TPO for 1 week. The *left panels* (*A*) are the total cell number of cultured AC133$^+$ cells from peripheral blood (*upper panel*) and cord blood (*lower panel*). The *right panels* (*B*) are the calculated CD31^{bright} cell number from peripheral blood (*upper panel*) and cord blood (*lower panel*). Columns and bars represent the means ± S.D. (**, $p < 0.01$; ***, $p < 0.001$). *Striped* and *dotted columns* represent CD31^{bright}VEcad$^+$ cells and CD31^{bright}VEcad$^-$ cells, respectively.

number of CD31^{bright} cells when compared with the control (Fig. 4*D*, *panel c*). The concomitant treatment with both VEGF and TPO showed a synergic increase in the number of CD31^{bright} cells (Fig. 4*D*, *panel c*).

When AC133$^+$ cells were cultured with various concentrations of TPO in the presence of constant concentrations of VEGF (50 ng/ml), the total cell number from both peripheral blood (Fig. 5*A*, *upper panel*) and cord blood (Fig. 5*A*, *lower panel*) significantly increased at 5 ng/ml of TPO when compared with the control, and there was no significant difference in the total cell number from 5 to 50 ng/ml of TPO. However, TPO increased the ratio of CD31^{bright} cells of flow cytometry dose-dependently as follows: control, 0.50%; 5 ng/ml, 1.36%; 10 ng, 1.42%; 50 ng/ml 1.90% in peripheral blood and control, 1.16%; 5 ng/ml, 1.99%; 10 ng, 2.51%; 50 ng/ml 2.96% in cord blood. TPO markedly induced the differentiation of AC133$^+$ cells into CD31^{bright}VEcad$^+$ cells in the case of both peripheral blood (Fig. 5*B*, *upper panel*) and cord blood (Fig. 5*B*, *lower panel*) in a dose-dependent manner. In the case of cord blood cells, differentiation into CD31^{bright}VEcad$^-$ cells was also induced by TPO.

The effects of TPO on total cell number during 6-day culture of AC133$^+$ cells were determined. Although the total cell num-

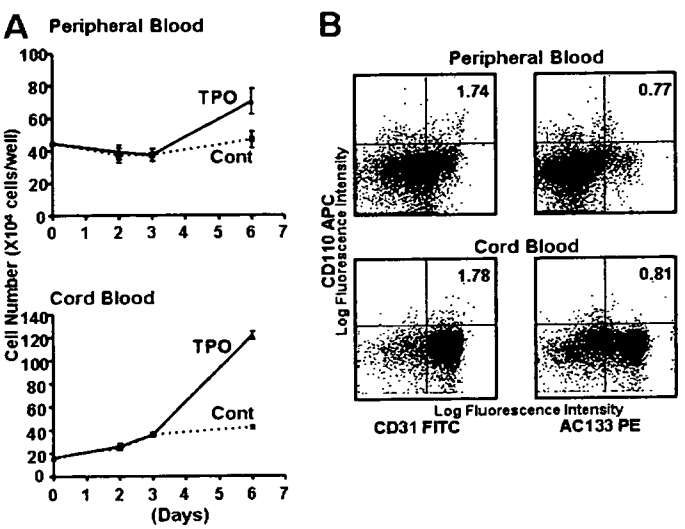

FIGURE 6. **Time-course analysis of TPO-treated AC133$^+$ cells and expression of TPO receptor (CD110).** *A*, alteration of cell number was counted at 2, 3, and 6 days. *Solid* and *dotted lines* indicate TPO-treated cells and control ((*Cont*) VEGF alone) cells, respectively. The results represent mean ± S.E. of triplicate wells. *B*, flow cytometric analysis of CD110 expression on AC133$^+$ cells cultured for 3 days was carried out. The *y axis* represents the log fluorescence intensity of CD110-allophycocyanin (*APC*), and the *x axis* represents that of CD31-FITC (*left panels*) and AC133-PE (*right panels*). The *number* in the flow cytometric dot blot indicates the percentage of CD110$^+$ CD31$^+$ and CD110$^+$ AC133$^+$ populations, respectively. The *upper panels* are peripheral blood, and the *lower panels* are cord blood.

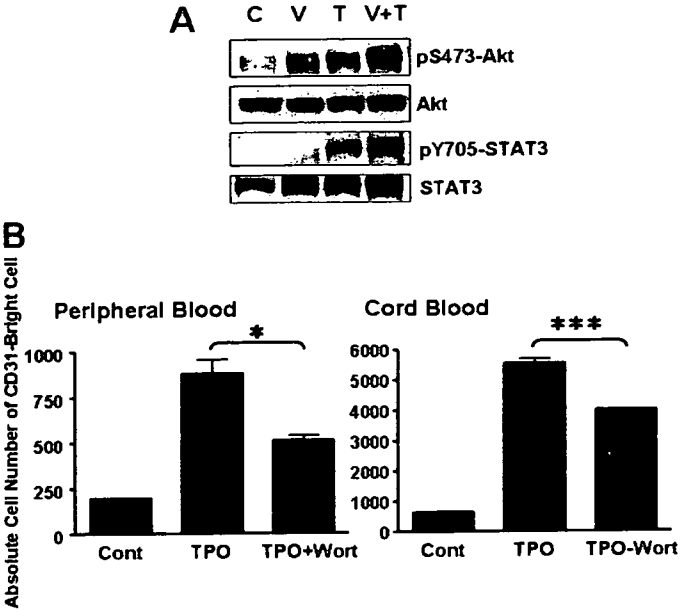

FIGURE 7. **Analysis of TPO-induced signal transduction on AC133$^+$ cells of cord blood.** *A*, activation of Akt or STAT3 was analyzed by Western blotting with anti-phospho-specific Ser-473-Akt antibody (*top panel*) and reprobed with anti-Akt antibody (*second panel*), or with anti-phospho-specific Tyr-705-STAT3 antibody (*third panel*) and reprobed with anti-STAT3 antibody (*lower panel*) after stimulation by VEGF, TPO, or both VEGF and TPO for 15 min using 3-day-cultured AC133$^+$ cells. *C*, control; *V*, VEGF; *T*, TPO. *B*, the effects of wortmannin on CD31^{bright} cell induction were investigated. The *right panel* shows peripheral blood, and the *left panel* shows cord blood. The *y axis* represents the CD31^{bright} cell number. *Wort*, 100 nM wortmannin. Columns and bars represent the means ± S.E. (*, $p < 0.05$; ***, $p < 0.001$). *Cont*, control.

ber from AC133$^+$ cells slightly and constantly increased from day 0 to day 6 in the absence of TPO, total cells markedly increased after the third day in the presence of TPO (Fig. 6*A*). Next, the alternation of TPO receptor (CD110) expression was analyzed during the cultivation of AC133$^+$ cells. Although the percentages of both AC133$^+$ CD110$^+$ cells and CD31$^+$ CD110$^+$ cells were 0% just after magnetic cell sorting, 3 days after the cultivation, ~2% of CD31$^+$ CD110$^+$ cells (Fig. 6*B*, *left panel*) and 1% of AC133$^+$ CD110$^+$ cells (Fig. 6*B*, *right panel*) appeared from AC133$^+$ cells in the peripheral blood and cord blood, respectively. These data indicate the possibility that sorted AC133$^+$ cells may differentiate into AC133$^+$ CD110$^+$ cells and may subsequently proliferate and differentiate into EPCs in response to TPO.

It has been reported that TPO activates the PI3K/Akt pathway (28) or JAK/STAT pathway (20, 29, 30) in target cells. In addition, in the present study, TPO induced a marked proliferation of AC133$^+$ cells after 3-day culture, and CD110 expression in cells cultured for 3 days from both cord blood and peripheral blood was also observed (Fig. 6, *A* and *B*). We then attempted to determine whether TPO activates Akt or STAT in AC133$^+$ cells cultured for 3 days by analyzing the phosphorylation at Ser-473 of Akt or the phosphorylation at Tyr-705 of STAT3, which are the active forms of Akt or STAT3, respectively. As shown in Fig. 7*A*, phosphorylation at Ser-473 of Akt was stimulated by both VEGF and TPO at 15 min and was more markedly stimulated by concomitant treatment with VEGF and TPO than by a single treatment (Fig. 7*A*, *top panel*). Phosphorylation at Tyr-705 of STAT3 was observed only in the presence of TPO, and unlike in the phosphorylation at Ser-473 of Akt, an increased amount of phosphorylation was not observed in the concomitant presence of VEGF and TPO (Fig. 7*A*, *third panel*). On the other hand, there was no difference in the expression of Akt and STAT3 protein levels (Fig. 7*A*, *second panel* and *bottom panel*, respectively). The induction of CD31^{bright} cells was not perfectly but significantly inhibited by wortmannin, an inhibitor of PI3K, suggesting that the PI3K/Akt pathway plays an important role in TPO-induced EPC differentiation (Fig. 7*B*).

DISCUSSION

We have previously reported that CD31^{bright} cells derived from AC133$^+$ cells in human peripheral blood are EPCs (25). In the present study, CD31^{bright} cells also appeared from AC133$^+$ cells prepared from cord blood, which are a rich source of stem cells during the early period of cultivation (Fig. 1, *A* and *B*). When cells were separated in terms of CD31 expression (Fig. 1*C*), CD31^{bright} cells differentiated into KDR-positive and eNOS-positive adherent cells. These data indicate that CD31^{bright} cells derived from AC133$^+$ cells in cord blood have some characteristics similar to those of EPCs in peripheral blood. Although these EPCs in both cord blood and peripheral blood could not form tube-like structure by themselves on Matrigel (data not shown), they secreted angiogenic growth factors (Fig. 2) such as VEGF, IL-8 (31, 32), and monocyte chemoattractant protein-1 (MCP-1) (33). It has been reported that there are at least two types of EPCs: early EPCs and late EPCs. Early EPCs are unable to form tube-like structures and secrete VEGF and IL-8 showing peak growth at 2–3 weeks (9, 26, 27). Late EPCs with the ability to proliferate and having a cobblestone shape appear late at 2–3 weeks, show exponential growth at 4–8 weeks, and have the ability to form tube-like structures

(26, 27, 34). Rehman *et al.* (9) have reported that EPCs derived from monocytes/macrophages do not proliferate but instead release potent proangiogenic growth factors. In many studies (9, 26, 27, 35–37), because the origin of early EPCs was $CD14^+$ cells or was not precluded by monocytic cells, CD14 expression was still observed in the EPCs after cultivation. In our study, in which $AC133^+$ cells were used as the origin of the EPCs, CD14 expression was not observed in $CD31^{bright}$ cells induced by TPO (Fig. 3*B*). Although the $CD31^{bright}$ cells identified as EPCs in this report and in a previous report did not correspond to their cells in terms of the origin of the cells or cell surface markers, these cells may be early EPCs that can release potent proangiogenic growth factors (Fig. 2). In any event, EPCs are thought to be a heterogeneous population, unlike late EPCs, which have a high ability to proliferate.

Circulating EPCs are up-regulated under physiological or pathological conditions and also by 3-hydroxy-3-methyl-glutaryl-CoA reductase inhibitors (14, 15) and cytokines such as erythropoietin (11–13) and G-CSF (10). In this report, we have revealed the possibility of marked expansion of EPCs *in vitro* by TPO. Brizzi *et al.* (20) have reported that TPO directly stimulates endothelial cell motility and neoangiogenesis. In the present study, TPO may have played a stimulatory role in the differentiation of EPCs from circulating stem cells.

Although both TPO and SCF have the same potency with regard to proliferation of $AC133^+$ cells (Fig. 4*A*), TPO specifically induces an increase in the ratio of the $CD31^{bright}$ cell population when compared with SCF (Fig. 4, *B* and *C*). To develop useful cell therapy products for severe ischemia, it has been considered desirable to establish the efficient expansion of EPCs *in vitro*. Thrombopoietin could increase $CD31^{bright}$ cells (EPCs) even in the absence of VEGF. Kirito *et al.* (38) have reported that TPO enhances expression of VEGF in hematopoietic cells through induction of hypoxia-inducible factor 1α. These observations suggest the possibility that the production of EPCs by TPO may be supported by VEGF produced by $AC133^+$ cells. However, from the perspective that TPO and VEGF have synergistic effects on the induction of EPCs, TPO seems to induce EPCs through another signaling cascade.

Thrombopoietin is a major regulator of the proliferation, differentiation, and maturation of megakaryocytes (39, 40). The results from recent studies suggest that TPO can act not only as a lineage-specific hematopoietic growth factor but also can affect other hematopoietic cell types. For example, TPO alone does not induce proliferation of long term repopulating hematopoietic stem cells. However, in combination with SCF or IL-3, TPO has several synergistic effects on cell proliferation (19). Our results have revealed a new role of TPO in the production of EPCs.

In the process of differentiation of $AC133^+$ cells into $CD31^{bright}$ cells, both peripheral blood and cord blood appear to be very similar. $AC133^+$ cells of cord blood, however, have a stronger ability to proliferate than those of peripheral blood (Fig. 6*A*). Moreover, TPO stimulates the induction of $CD31^{bright}VEcad^-$ cells only from cord blood (Fig. 5*B*) at high concentrations. Hur *et al.* (26) have reported that $VEcad^-$ EPCs are thought to be an early EPC. It is therefore thought that $AC133^+$ cells of cord blood are more immature than those of peripheral blood.

Although the total cell number treated with TPO slightly increased in a dose-dependent manner (Fig. 5*A*), the $CD31^{bright}$ cell number markedly increased as the TPO concentration increased (Fig. 5*B*). These data suggest the possibility that a higher concentration of TPO may be needed for $CD31^{bright}$ cell induction from $AC133^+$ cells.

When $AC133^+$ cells were stimulated by TPO or VEGF, an increase in the phosphorylation of Akt at Ser-473 was observed. This increase was strongly enhanced by concomitant treatment with VEGF and TPO (Fig. 7*A*). The induction of $CD31^{bright}$ cells by these growth factors (Fig. 4*D*) was consistent with the increase in the phosphorylation of Akt at Ser-473. TPO but not VEGF could also stimulate the phosphorylation of STAT3 at Tyr-705. We previously reported that the PI3K/p70 S6 kinase pathway and the JAK/STAT3 pathway were important for proliferation and differentiation, respectively, in neutrophilic differentiation (41, 42). Owing to the stimulation of both the PI3K/Akt and the JAK/STAT pathways, we postulated that TPO may be a stronger stimulator of EPC production than VEGF. As shown in Fig. 7*B*, however, wortmannin could not completely inhibit the induction of $CD31^{bright}$ cells. Therefore, a pathway other than the PI3K/Akt pathway may also work for the proliferation and differentiation of EPCs.

The observation of unfavorable angiogenesis has recently been reported after transplantation of bone marrow mononuclear cells in patients with thromboangiitis obliterans (43). Moreover, transfer of both spleen cell-derived EPCs and bone marrow mononuclear cells accelerate atherosclerosis in apoE knockout mice, whereas EPC transfer reduces markers associated with plaque stability (44). These observations suggest that transplantation of differentiated cells from EPCs may be useful therapy as regenerative medicine.

In conclusion, we have demonstrated a new role of TPO in enhancing the differentiation of $AC133^+$ cells into $CD31^{bright}$ cells (EPCs) *in vitro*. These findings may contribute to further development of cell therapy for critical ischemia.

Acknowledgments—We thank Saitama Red Cross of Japan (Saitama, Japan) and Metro Tokyo Red Cross Cord Blood Bank (Tokyo, Japan) for their kind cooperation. We also thank Kirin-Amgen Inc. for their kind gift of recombinant TPO and recombinant SCF.

REFERENCES

1. Asahara, T., Masuda, H., Takahashi, T., Kalka, C., Pastore, C., Silver, M., Kearne, M., Magner, M., and Isner, J. M. (1999) *Circ. Res.* **85,** 221–228
2. Asahara, T., Murohara, T., Sullivan, A., Silver, M., van der Zee, R., Li, T., Witzenbichler, B., Schatteman, G., and Isner, J. M. (1997) *Science* **275,** 964–967
3. Asahara, T., Takahashi, T., Masuda, H., Kalka, C., Chen, D., Iwaguro, H., Inai, Y., Silver, M., and Isner, J. M. (1999) *EMBO J.* **18,** 3964–3972
4. Shi, Q., Rafii, S., Wu, M. H., Wijelath, E. S., Yu, C., Ishida, A., Fujita, Y., Kothari, S., Mohle, R., Sauvage, L. R., Moore, M. A., Storb, R. F., and Hammond, W. P. (1998) *Blood* **92,** 362–367
5. Takahashi, T., Kalka, C., Masuda, H., Chen, D., Silver, M., Kearney, M., Magner, M., Isner, J. M., and Asahara, T. (1999) *Nat. Med.* **5,** 434–438
6. Nieda, M., Nicol, A., Denning-Kendall, P., Sweetenham, J., Bradley, B., and Hows, J. (1997) *Br. J. Haematol.* **98,** 775–777
7. Gill, M., Dias, S., Hattori, K., Rivera, M. L., Hicklin, D., Witte, L., Girardi, L., Yurt, R., Himel, H., and Rafii, S. (2001) *Circ. Res.* **88,** 167–174
8. Peichev, M., Naiyer, A. J., Pereira, D., Zhu, Z., Lane, W. J., Williams, M.,

Oz, M. C., Hicklin, D. J., Witte, L., Moore, M. A., and Rafii, S. (2000) *Blood* **95,** 952–958
9. Rehman, J., Li, J., Orschell, C. M., and March, K. L. (2003) *Circulation* **107,** 1164–1169
10. Kocher, A. A., Schuster, M. D., Szabolcs, M. J., Takuma, S., Burkhoff, D., Wang, J., Homma, S., Edwards, N. M., and Itescu, S. (2001) *Nat. Med.* **7,** 430–436
11. Bahlmann, F. H., De Groot, K., Spandau, J. M., Landry, A. L., Hertel, B., Duckert, T., Boehm, S. M., Menne, J., Haller, H., and Fliser, D. (2004) *Blood* **103,** 921–926
12. Bahlmann, F. H., DeGroot, K., Duckert, T., Niemczyk, E., Bahlmann, E., Boehm, S. M., Haller, H., and Fliser, D. (2003) *Kidney Int.* **64,** 1648–1652
13. Heeschen, C., Aicher, A., Lehmann, R., Fichtlscherer, S., Vasa, M., Urbich, C., Mildner-Rihm, C., Martin, H., Zeiher, A. M., and Dimmeler, S. (2003) *Blood* **102,** 1340–1346
14. Dimmeler, S., Aicher, A., Vasa, M., Mildner-Rihm, C., Adler, K., Tiemann, M., Rutten, H., Fichtlscherer, S., Martin, H., and Zeiher, A. M. (2001) *J. Clin. Investig.* **108,** 391–397
15. Llevadot, J., Murasawa, S., Kureishi, Y., Uchida, S., Masuda, H., Kawamoto, A., Walsh, K., Isner, J. M., and Asahara, T. (2001) *J. Clin. Investig.* **108,** 399–405
16. Kaushansky, K., Lok, S., Holly, R. D., Broudy, V. C., Lin, N., Bailey, M. C., Forstrom, J. W., Buddle, M. M., Oort, P. J., Hagen, F. S., Roth, G. J., Papayannopoulou, T., and Foster, D. C. (1994) *Nature* **369,** 568–571
17. Fox, N., Priestley, G., Papayannopoulou, T., and Kaushansky, K. (2002) *J. Clin. Investig.* **110,** 389–394
18. Kimura, S., Roberts, A. W., Metcalf, D., and Alexander, W. S. (1998) *Proc. Natl. Acad. Sci. U. S. A.* **95,** 1195–1200
19. Sitnicka, E., Lin, N., Priestley, G. V., Fox, N., Broudy, V. C., Wolf, N. S., and Kaushansky, K. (1996) *Blood* **87,** 4998–5005
20. Brizzi, M. F., Battaglia, E., Montrucchio, G., Dentelli, P., Del Sorbo, L., Garbarino, G., Pegoraro, L., and Camussi, G. (1999) *Circ. Res.* **84,** 785–796
21. Kaushansky, K., Lin, N., Grossmann, A., Humes, J., Sprugel, K. H., and Broudy, V. C. (1996) *Exp. Hematol.* **24,** 265–269
22. Broudy, V. C., Lin, N. L., and Kaushansky, K. (1995) *Blood* **85,** 1719–1726
23. Kaushansky, K., Broudy, V. C., Grossmann, A., Humes, J., Lin, N., Ren, H. P., Bailey, M. C., Papayannopoulou, T., Forstrom, J. W., and Sprugel, K. H. (1995) *J. Clin. Investig.* **96,** 1683–1687
24. Kobayashi, M., Laver, J. H., Kato, T., Miyazaki, H., and Ogawa, M. (1995) *Blood* **86,** 2494–2499
25. Kanayasu-Toyoda, T., Yamaguchi, T., Oshizawa, T., and Hayakawa, T. (2003) *J. Cell. Physiol.* **195,** 119–129
26. Hur, J., Yoon, C. H., Kim, H. S., Choi, J. H., Kang, H. J., Hwang, K. K., Oh, B. H., Lee, M. M., and Park, Y. B. (2004) *Arterioscler. Thromb. Vasc. Biol.* **24,** 288–293
27. Yoon, C. H., Hur, J., Park, K. W., Kim, J. H., Lee, C. S., Oh, I. Y., Kim, T. Y., Cho, H. J., Kang, H. J., Chae, I. H., Yang, H. K., Oh, B. H., Park, Y. B., and Kim, H. S. (2005) *Circulation* **112,** 1618–1627
28. Miyakawa, Y., Rojnuckarin, P., Habib, T., and Kaushansky, K. (2001) *J. Biol. Chem.* **276,** 2494–2502
29. Drachman, J. G., Sabath, D. F., Fox, N. E., and Kaushansky, K. (1997) *Blood* **89,** 483–492
30. Kirito, K., Watanabe, T., Sawada, K., Endo, H., Ozawa, K., and Komatsu, N. (2002) *J. Biol. Chem.* **277,** 8329–8337
31. Li, A., Dubey, S., Varney, M. L., Dave, B. J., and Singh, R. K. (2003) *J. Immunol.* **170,** 3369–3376
32. Mizukami, Y., Jo, W. S., Duerr, E. M., Gala, M., Li, J., Zhang, X., Zimmer, M. A., Iliopoulos, O., Zukerberg, L. R., Kohgo, Y., Lynch, M. P., Rueda, B. R., and Chung, D. C. (2005) *Nat. Med.* **11,** 992–997
33. Salcedo, R., Ponce, M. L., Young, H. A., Wasserman, K., Ward, J. M., Kleinman, H. K., Oppenheim, J. J., and Murphy, W. J. (2000) *Blood* **96,** 34–40
34. Lin, Y., Weisdorf, D. J., Solovey, A., and Hebbel, R. P. (2000) *J. Clin. Investig.* **105,** 71–77
35. Assmus, B., Schachinger, V., Teupe, C., Britten, M., Lehmann, R., Dobert, N., Grunwald, F., Aicher, A., Urbich, C., Martin, H., Hoelzer, D., Dimmeler, S., and Zeiher, A. M. (2002) *Circulation* **106,** 3009–3017
36. Kalka, C., Masuda, H., Takahashi, T., Kalka-Moll, W. M., Silver, M., Kearney, M., Li, T., Isner, J. M., and Asahara, T. (2000) *Proc. Natl. Acad. Sci. U. S. A.* **97,** 3422–3427
37. Kawamoto, A., Gwon, H. C., Iwaguro, H., Yamaguchi, J. I., Uchida, S., Masuda, H., Silver, M., Ma, H., Kearney, M., Isner, J. M., and Asahara, T. (2001) *Circulation* **103,** 634–637
38. Kirito, K., Fox, N., Komatsu, N., and Kaushansky, K. (2005) *Blood* **105,** 4258–4263
39. Kelemen, E., Cserhati, I., and Tanos, B. (1958) *Acta Haematol. (Basel)* **20,** 350–355
40. Yamamoto, S. (1957) *Acta Haematol. Jpn.* **20,** 163
41. Kanayasu-Toyoda, T., Yamaguchi, T., Uchida, E., and Hayakawa, T. (1999) *J. Biol. Chem.* **274,** 25471–25480
42. Yamaguchi, T., Mukasa, T., Uchida, E., Kanayasu-Toyoda, T., and Hayakawa, T. (1999) *J. Biol. Chem.* **274,** 15575–15581
43. Miyamoto, K., Nishigami, K., Nagaya, N., Akutsu, K., Chiku, M., Kamei, M., Soma, T., Miyata, S., Higashi, M., Tanaka, R., Nakatani, T., Nonogi, H., and Takeshita, S. (2006) *Circulation* **114,** 2679–2684
44. George, J., Afek, A., Abashidze, A., Shmilovich, H., Deutsch, V., Kopolovich, J., Miller, H., and Keren, G. (2005) *Arterioscler. Thromb. Vasc. Biol.* **25,** 2636–2641

Leukemia (2007), 1–10

www.nature.com/leu

ORIGINAL ARTICLE

Proteome analyses of the growth inhibitory effects of NCH-51, a novel histone deacetylase inhibitor, on lymphoid malignant cells

T Sanda[1,2], T Okamoto[1], Y Uchida[1], H Nakagawa[3], S Iida[2], S Kayukawa[2], T Suzuki[3], T Oshizawa[4], T Suzuki[4], N Miyata[3] and R Ueda[2]

[1]*Department of Molecular and Cellular Biology, Nagoya City University Graduate School of Medical Sciences, Nagoya, Japan;* [2]*Department of Internal Medicine and Molecular Science, Nagoya City University Graduate School of Medical Sciences, Nagoya, Japan;* [3]*Department of Organic and Medicinal Chemistry, Nagoya City University Graduate School of Pharmaceutical Sciences, Nagoya, Japan and* [4]*Department of Cellular and Gene Therapy Products, National Institute of Health Sciences, Tokyo, Japan*

Recent reports showing successful inhibition of cancer and leukemia cell growth using histone deacetylase inhibitor (HDACi) compounds have highlighted the potential use of HDACi as anti-cancer agents. However, high incidence of toxicity and low stability *in vivo* were observed with hydroxamic acid-based HDACi such as suberoylanilide hydroxamic acid (SAHA), thus limiting its clinical applicability. In this study, we found that a novel non-hydroxamate HDACi NCH-51 could inhibit the cell growth of a variety of lymphoid malignant cells through apoptosis induction, more effectively than SAHA. Activation of caspase-3, -8 and -9, but not -7 was detected after the treatment with NCH-51. Gene expression profiles showed that NCH-51 and SAHA similarly upregulated *p21* and downregulated anti-apoptotic molecules including *survivin*, *bcl-w* and *c-FLIP*. Proteome analysis using two-dimensional electrophoresis revealed that NCH-51 upregulated anti-oxidant molecules including peroxiredoxin 1 and 2 and glutathione *S*-transferase at the protein level. Interestingly, NCH-51 induced reactive oxygen species (ROS) after 8 h whereas SAHA continuously declined ROS. Pretreatment with an antioxidant, *N*-acetyl-L-cysteine, abolished the cytotoxicity of NCH-51. These findings suggest that NCH-51 exhibits cytotoxicity by sustaining ROS at the higher level greater than SAHA. This study indicates the therapeutic efficacy of NCH-51 and novel insights for anti-HDAC therapy.
Leukemia advance online publication, 9 August 2007;
doi:10.1038/sj.leu.2404902
Keywords: histone deacetylase; apoptosis; reactive oxygen species; peroxiredoxin

Introduction

Histone deacetylase (HDAC) is responsible for deacetylation of histone or non-histone substrates.[1–3] Deacetylation of histone converts local chromatin into repressive configuration, resulting in the transcriptional repression.[2,3] The aberrant recruitment of HDAC is closely associated with leukemogenesis through silencing of expression of the genes involved in hematopoietic cell differentiation.[4] In addition, subsequent studies demonstrated that the malignant phenotypes of solid tumors could be ascribed to the aberrant activation of HDAC and deacetylation of the histone proteins adjacent to tumor suppressor genes.[5,6] Thus, a number of small-molecule HDAC inhibitors (HDACi) have been developed as anti-cancer agents.[1,7] In fact, HDACi compounds were shown to induce cell cycle arrest, differentiation and apoptosis in a variety of malignant cells.[1,7]

Suberoylanilide hydroxamic acid (SAHA) (also known as vorinostat) belongs to a hydroxamic acid-based hybrid polar compound and is a prototypic compound of HDACi.[7] Phase I clinical trials with refractory solid tumors and hematological malignancies by SAHA revealed frequent toxicities including dehydration, fatigue, diarrhea, anorexia and cytopenia, in spite of significant clinical benefits.[8] In addition, a poor pharmacokinetics of SAHA was noted.[8] Other hydroxamic acid-based derivatives showed similar therapeutic profiles.[9,10] Thus, we have attempted to develop a non-hydroxamate HDACi to overcome these problems. A novel HDACi NCH-51 was designed based on SAHA by replacement of the hydroxamic acid by acylated thiol group. NCH-51 could inhibit HDACs as strongly as SAHA and inhibited the cell growth of various solid tumor cell lines *in vitro* (mean IC_{50} values of NCH-51 and SAHA are 3.8 and 3.7 μM, respectively).[11] Unlike SAHA, NCH-51 is stable in human plasma at the remaining rate of approximately 51% after 24 h of administration (unpublished data).

Recent findings suggest that HDACi may have additional effects other than transcriptional interference. Although it is well established that HDACi upregulates gene expression of tumor suppressors such as *p21* through histone hyperacetylation,[12–14] HDACi does not always upregulate gene expression but induces malignant cell death by downregulating gene expression such as anti-apoptotic genes. In addition, some HDACi compounds exhibited anti-cancer effects through acetylation of non-histone substrates such as heat-shock protein 90 (HSP90),[15] α-tubulin,[16] p53[17] and nuclear factor-κB.[18] For example, Bali *et al.*[15] reported that HDACi caused leukemia cell death by hyperacetylation of HSP90. Hideshima *et al.*[19] demonstrated that tubacin, a specific HDAC6 inhibitor, was effective in augmenting cell death mediated by bortezomib, a proteasome inhibitor, by inhibiting the protein degradation through blocking aggresome activity. Thus, the cell growth inhibitory action of HDACi could be exhibited at the protein expression level.

Here we demonstrate the therapeutic efficacy of NCH-51 on lymphoid malignant cells. NCH-51 induced cell death, more strongly than SAHA. We analyzed the protein expression profiles and found that NCH-51 modulated the expression of antioxidant molecules at the protein level. NCH-51 sustained the intracellular reactive oxygen species (ROS) greater than SAHA.

Correspondence: Professor T Okamoto, Department of Molecular and Cellular Biology, Nagoya City University Graduate School of Medical Sciences, 1 Kawasumi, Mizuho-cho, Mizuho-ku, Nagoya, Aichi 467-8601, Japan.
E-mail: tokamoto@med.nagoya-cu.ac.jp
Received 22 March 2007; revised 6 June 2007; accepted 11 July 2007

a

Cell type		Cell line name	24h		72h	
			SAHA	NCH-51	SAHA	NCH-51
T-cell	T-ALL	Jurkat	0.90	0.72	0.63	0.75
	ATL	MT-2	>30.00		0.54	2.08
		ATL-102	>30.00		3.70	2.25
		ED-40515 (-)		0.94	0.90	0.76
	CLL	MEC2	>30.00	0.71	0.70	0.67
		MO1043	>30.00		0.76	0.79
B-cell	BL	Raji	>30.00	1.65	0.84	0.71
		Daudi	>30.00	>30.00		
	MM	U266		1.36	0.53	0.66
		XG7	>30.00		0.73	1.11
		KMS	>30.00		1.35	3.49
		ILKM-2	1.41	1.11	0.61	0.66
		RPMI8226		2.92	2.92	2.72

Growth inhibition (%)
80-100
60-80
40-60
20-40
0-20

Each Value means IC_{50}

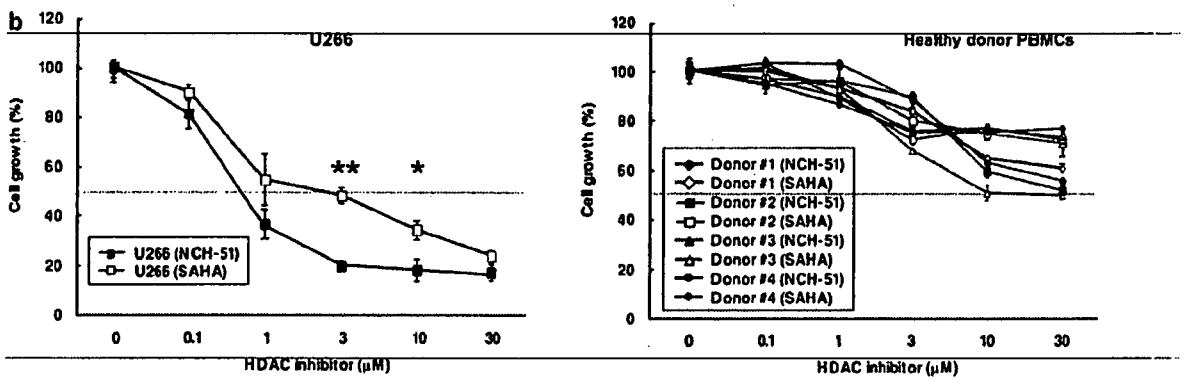

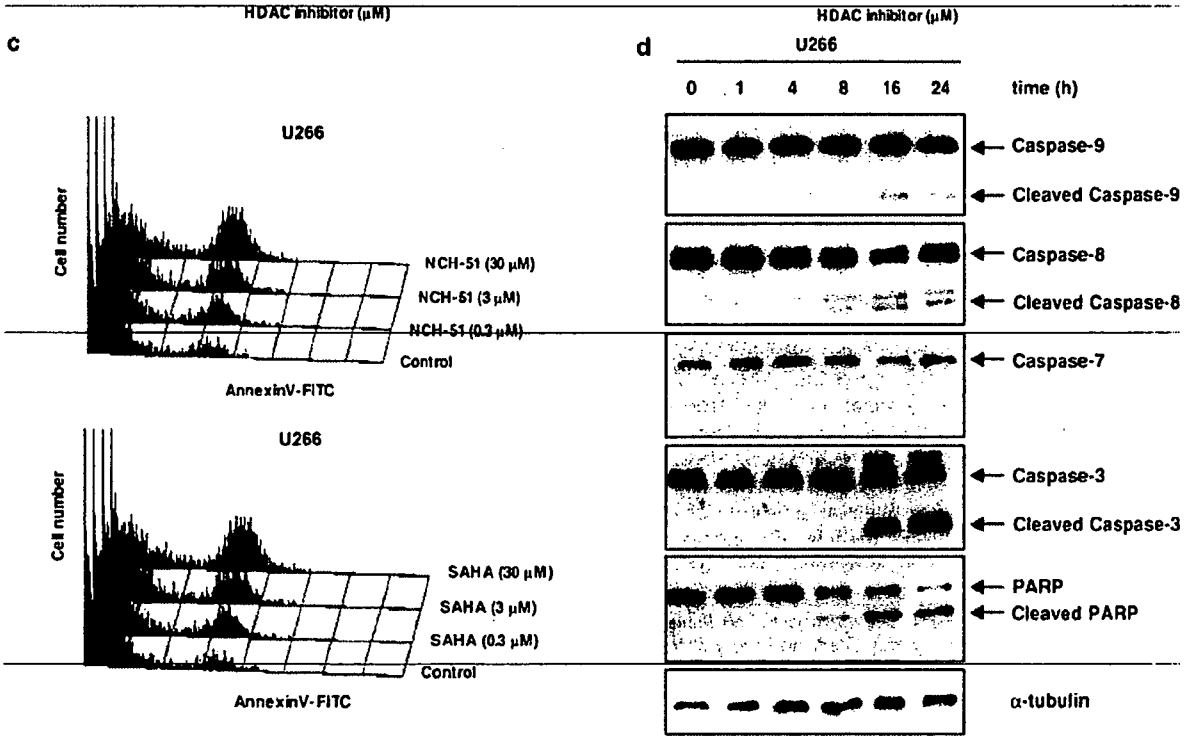

Materials and methods

Cell lines and reagents

A human acute T-cell leukemia cell line, Jurkat, ATL cell lines, MT-2, ATL-102 and ED-40515(−), chronic lymphocytic leukemia cell lines, MEC2 and MO1043, Burkitt's lymphoma cell lines, Raji and Daudi and multiple myeloma cell lines, U266, XG7, KM5, ILKM-2 and RPMI-8226 were used in this study as described previously.[20–24] For normal controls, peripheral blood mononuclear cells (PBMCs) were obtained from four independent healthy donors upon informed consent after the approval of Institutional Ethical Committee. All cells were cultured in RPMI-1640 medium, supplemented with 10% fetal bovine serum at 37°C in a 5% CO_2 incubator. NCH-51, a novel non-hydroxamate HDACi, and SAHA, a conventional hydroxamate HDACi, were synthesized by us as described previously.[11] NCH-51 and SAHA were dissolved in dimethyl sulfoxide at 50 mM and stored at −20°C. An antioxidant compound *N*-acetyl-L-cysteine (NAC) was purchased from Sigma (St Louis, MS, USA).

Growth inhibition assay

Growth inhibitory effect of HDACi was determined using 3-(4,5-dimethylthiazol-2-yl)-2,5-diphenyltetrazolium bromide assay (Sigma) as described previously.[25] Briefly, approximately $1–10 \times 10^4$ cells per 100 μl were cultured in 96-well plate in triplicates at 37°C. Optical densities (OD) at 570 and 630 nm were measured with a multiplate reader. Cell growth (%) was calculated as follows: (OD_{630}–OD_{570} of the samples/OD_{630}–OD_{570} of the control) × 100.

Apoptosis and cell cycle analysis

Apoptosis and cell cycle analyses were performed as described previously.[20] For apoptosis analysis, the cells were treated with or without HDACi for 18 h, and incubated with fluorescein isothiocyanate (FITC)-conjugated annexin V (MBL, Nagoya, Japan). The cell numbers of annexin V-positive cells were analyzed by flowcytometry (FACScan, BD Bioscience, San Jose, CA, USA) and CellQuest analysis program (BD Bioscience). For cell cycle analysis, the cells were incubated with or without HDACi for 24 h, washed with cold phosphate-buffered saline (PBS), and fixed with 70% ethanol. After incubation with RNase A (Qiagen, Alameda, CA, USA), the cell pellets were resuspended in PBS containing propidium iodide (Sigma). DNA content of each cell preparation was analyzed by flowcytometry.

Protein extraction for proteome analysis

Proteome analysis was performed according to Seike *et al.*[26] U266 cells were incubated with or without 3 μM NCH-51 for 18 h. The cell pellets were washed with cold PBS and then treated with 10%trichloroacetic acid for 30 min on ice. After washing with PBS, the pellets were collected and resuspended in lysis buffer (30 mM Tris–HCl (pH, 8.5), 7 M urea, 2 M thiourea, 3% 3-((3-chlamidopropyl) dimethylammonio)-1-propanesulfonic acid and 1% Triton X-100). Samples were then subjected to a Dounce homogenizer for 30 strokes and sonicated for 5 min in a sonicator (UCW-201, Cosmobio Co. Ltd., Tokyo, Japan). After incubation for 30 min, the samples were centrifuged at 10 000 × *g* for 30 min followed by ultracentrifugation at 100 000 × *g* for 1 h, and the supernatants were collected. Protein concentration was determined by 2D-Quant kit (GE Healthcare Bio-Sciences Corp., Piscataway, NJ, USA). Fifty micrograms of each protein extract, adjusted to pH 8.5, were labeled with 200 pmol of minimal dye CyDye (GE Healthcare Bio-Sciences Corp.). NCH-51-treated samples and untreated control proteins were labeled with Cy3 and Cy5, respectively. Internal control, consisting of half part of each paired sample was labeled with Cy2. Labeling reaction was stopped with the addition of 0.2 mM L-lysine (Sigma) for 10 min on ice. Each labeled sample was mixed into one tube and then incubated with an equal amount of lysis buffer for 10 min on ice. The final volume was adjusted to 450 μl with DeStreak Rehydration Solution and 0.5% IPG buffer (GE Healthcare Bio-Sciences Corp.).

Two-dimensional (2D) electrophoresis and image analysis

An immobilized pH gradient gel Immobiline DryStrip (GE Healthcare Bio-Sciences Corp.), with non-linear pH values (3–10), was rehydrated with the labeled protein samples at 20°C for 12 h. Isoelectric focusing was performed using IPGphor (GE Healthcare Bio-Sciences Corp.) at 20°C for total 65 000 khT. Immobiline DryStrips were then equilibrated for 15 min in the buffer (6 M urea, 1.5 M Tris–HCl (pH 8.8), 30% glycerol, 2% sodium dodecyl sulfate) containing 10 mg/ml dithiothreitol and prolonged for 15 min in the same buffer containing 25 mg/ml iodoacetamide. After equilibration, Immobiline DryStrips were transferred onto 11.5% polyacrylamide gels and run in the EttanDalt Six system (GE Healthcare Bio-Sciences Corp.) at 30 W/gel for 5 h at 20°C. The gels were scanned with appropriate wavelengths for excitation and emission using Ettan DIGE Primo (GE Healthcare Bio-Sciences Corp.). Relative quantification of spot intensities and statistical evaluation were carried out with ImageMaster 2D Platinum software (GE Healthcare Bio-Sciences Corp.). The experiments were performed in quadruplicates. The protein spots that were statisti-

Figure 1 Induction of apoptosis by a novel HDAC inhibitor NCH-51. (**a**) The growth inhibitory effects of NCH-51 and suberoylanilide hydroxamic acid (SAHA) on 13 lymphoid malignant cell lines. The cells were treated with either NCH-51 or SAHA (3 μM) for 24 or 72 h. Cell growth was estimated by 3-(4,5-dimethylthiazol-2-yl)-2,5-diphenyltetrazolium bromide (MTT) assay and gray-scale levels represent the growth inhibition rate (%) compared to untreated control. Each value indicates the mean IC_{50}. (**b**) Growth inhibitory effects of NCH-51 and SAHA on U266 cells and four control peripheral blood mononuclear cells (PBMCs). A multiple myeloma cell line U266 cells, and four healthy donor PBMCs were treated with indicated concentrations (0–30 μM) of NCH-51 (closed symbols) or SAHA (opened symbols) for 24 h. Cell growth was evaluated by MTT assay. The results are shown as the percentage cell growth compared to untreated control. These experiments were performed in triplicates and the mean values ± s.d. are shown. *$P<0.05$; **$P<0.01$. (**c**) Induction of apoptosis by NCH-51. U266 cells were treated with the indicated concentrations (0–30 μM) of NCH-51 for 18 h, stained with fluorescein isothiocyanate-conjugated annexin V, and analyzed by flowcytometry. Annexin V-positive fraction indicates the cells undergoing apoptosis. (**d**) Activation of caspases and poly-ADP ribose polymerase (PARP) cleavage by NCH-51. U266 cells were treated with 3 μM of NCH-51 for 0–24 h. Whole cell extracts were prepared and subjected to immunoblots with the indicated antibodies. Positions of uncleaved (inactivated) and cleaved (activated) caspases and PARP proteins are indicated by arrows.